Master's Thesis

Energy scavenging for medical applications

By

Petter Cederholm

LTH Supervisor: Anders J Johansson

Department of Electrical and Information Technology
Faculty of Engineering, LTH, Lund University
SE-221 00 Lund, Sweden

Abstract

This report was written with the intention to compile the existing methods for energy scavenging and to evaluate the feasibility of scavenging for energy for human implants. Energy scavenging - or energy harvesting - is the method used to collect, transform and use ambient energy. The amount of energy is assumed to be small. Typically applications are wireless autonomous sensor networks. The limitation was set to scavenging for circuitry used in medical applications; due to this was the motivation to this work. Ambient energy is defined as energy that is already present in the surrounding. Scavenging does thus not rely on any kind of fuel or stored energy.

The report is made up of two sections. The first is a compilation of scientific articles, which is categorized by physic source of energy: Motion and vibration, Radio frequency, Light and Thermal gradients. A thorough study was made, and the articles considered the most promising was chosen and reviewed. To evaluate the possibility of using motion based generators, a physical model of a generator was mathematically analyzed, along with generators tested on actual human conditions. To investigate the feasibility of scavenging for energy from radio frequency signals, measurements of the power densities in different environments, at different distances from the nearest base station under normal traffic was made. As for light as energy source, the efficiency of a solar cell was reviewed, and the radiation at ground level and at different depth under the skin estimated. The last energy source examined was thermal gradients. A model of a thermoelectric generator was mathematically analyzed, and figures of merit were provided. Furthermore, a section about driver electronics was added to provide figures of merit for power consumption. Material was mainly gathered from the Electronic Library Information Navigator, ELIN.

In the second section, a small circuit was implemented from the method found most useful for scavenging. This was implemented using an AVR microcontroller and other commonly available components. The system is described in detail and its performance analyzed, and its possible improvements are proposed.

Preface

The motivation for this work was the need of a study of the existing research in the field of energy scavenging. The work is meant to lie as basis for a work carried out at the EIT department at Lunds Tekniska Högskola in Lund, Sweden. This motive work concern design and implementation of so called brain machine interfaces, BMI. A BMI allows for communication with the central nervous system, making it possible to study neuronal mechanisms. The BMI communicates via implanted electrode arrays, and it is here the motivation arises. Due to the inherent complexity associated with changing the implants with a surgery, it is desired to avoid doing this too often. By extending the battery lifetime, the surgery time interval can be increased, with the resulting decreased risk and discomfort for the patient. It was therefore interesting to investigate whether energy scavenging could be a feasible way of extending the battery life time for these devices.

The gathering of information for this work was mainly made during the summer of 2010. The compilation was written in 2011 in Lund as a master thesis in Elektroteknik at Lunds Tekniska Högskola.

Table of contents

Abstract..... 2

Preface..... 3

Table of contents..... 4

Introduction..... 6

Method..... 6

Aim..... 7

Section I. Overview of the area..... 8

Motion and vibrations..... 8

Modeling..... 8

Implementation..... 12

Discussion..... 16

Radio frequency signals..... 19

RF levels in Europe..... 19

Implementation..... 21

Discussion..... 24

Light..... 25

Efficiency..... 25

MPPT..... 27

Implementation..... 28

Discussion..... 30

Thermal gradients..... 32

Modeling..... 32

Implementation..... 35

Discussion..... 39

Driver electronics..... 40
Discussion..... 42
Conclusions..... 43
Section II A scavenger circuit..... 45
Components..... 45
Working principle..... 48
Performance..... 52
Improvements..... 55
Conclusion..... 56
Section III..... 57
References..... 57
Appendix..... 60
1. Scavenger hardware..... 60
2. Scavenger board closeup..... 61
3. Scavenger board backside..... 61
4. Source code..... 62

Introduction

Energy scavenging is the collecting and storage of energy present in the surrounding. It does not use or rely on any kind of fuel or pre-stored energy, but rather collects the ambient stray energy that otherwise would go to waste. This area has lately become fast growing, mostly due to the increased use of small, wireless, low-power sensors networks. This technique is thus a promising way to contribute to powering such small system for in theory an infinite time, or at least vastly extend the battery life time.

In this work, focus is put on scavenging methods possible to use in medical applications. The work will investigate whether scavenging could be used as part of the power supply of a human implant. The first section is the theoretical part, consisting of a compilation of scientific articles on the topic. Each of the energy sources (motion, radio frequency signals, light and temperature gradients) are covered one by one. Mathematical modeling of the different systems is made were applicable, and estimations as well as practical results obtained are reported. Conclusions are then drawn about the method's prospects of usage in scavenging for ambient energy, and the most important result are summarized.

In the second section, a solar cell based scavenger is presented. This source was chosen based on the most promising energy source found in section 1, and experiences from here are used. The final circuit is described in detail and then analyzed by performance.

Method

The main part of this thesis is a theoretical compilation. The material for this study was mainly fetched from the Electronic Library Information Navigator, ELIN. All articles and conference papers with keywords energy scavenging/harvesting was downloaded. From this large amount of material, the most relevant information was sorted out in two-stage sorting process. In the first round, material with no actual contribution was sorted out. Typically those articles didn't have energy scavenging as main topic, but rather mentioned that harvesting could be used as part of the power

source, at concept level. After this first sorting, left was a number of papers each one containing useful information about energy scavenging. However, many of these articles covered each other, presenting the same information multiple times. Few of them covered energy harvesting in a lager scale, not applicable for medical applications, eg such as sea-based electrical power generation. These were hence rejected. Several articles described the building of actual generators, useful for medical applications. Since the aim of this thesis was to explore whether energy scavenging could be of use to powering human implants, the performance of these generators tested on actual human conditions was of high interest. After the second sorting round, a number of articles remained which effectively covered the most promising results in ELIN. These articles are summarized in the first part of this thesis.

When additional information was needed, either course literature was used or the internet was searched for reliable information. Wikipedia references was rejected due to their inconsistency.

As for the second part, a concept of optimizing the loading of a solar cell was brainstormed. The algorithm was implemented on an AVR microcontroller, using AVR Studio 4 for development.

Aim

This work was motivated by the need to investigate the current research status on the topic energy scavenging. Hence, the aim for this work was to make a thorough study of the topic and put it together in an easily accessible reference. It should contain detailed information about the different energy sources as well as the figures useful to decide if energy scavenging can be used for powering implants. By reading it, the reader should also get an introduction to the topic, and hopefully a sense of the whole concept by gaining knowledge about the different parts used in a scavenger.

Section I. Overview of the area

To investigate whether the concept of energy scavenging is a feasible way of being a part of the power supply of modern electronics, different methods for extracting energy will here be studied and evaluated. In the research of the subject there has traditionally been made a division accordingly to the physical source of energy. This compilation follows that pattern, and hence the sources as presented below are Motion and vibrations, Radio frequency signals, Light and Thermal gradients.

Motion and vibrations

Vibrations are common in a variety of areas (industrial, domestic, on a human etc.) and are therefore interesting to investigate with respect to its power content. Energy scavengers that utilize ambient vibrations are reasonable simple to construct, and there are even a few commercial gadgets on the market that uses this kind of motion for energy extraction. Though, due to the random-like motion available on a human, and the vast variations among people, it is hard to do meaningful simulations and calculations of this. For real life estimations, focus has therefore been put at evaluating the results of real systems tested on actual humans moving.

First in this section is presented a model that will lead to an expression for the extracted energy from a moving system. After that follows detailed descriptions of few scavengers that is built with the purpose of scavenging for human motion power. Last follows a discussion about the feasibility of using this energy source for energy harvesting in medical applications.

Modeling

Consider the spring-mass system in Fig 1 [1]. A proof mass m is connected to an outer frame with a spring with spring constant k, an electromechanical damping coefficient b_e and a mechanical coefficient b_m. The mechanical damping will represent mechanical losses.

The system will satisfy the differential equation

$$m\frac{d^2x(t)}{dt^2}+(b_e+b_m)\frac{dx(t)}{dt}+kx(t)=-m\frac{d^2y(t)}{dt^2} \quad , \tag{1}$$

were $x(t)$ is the proof mass displacement relative to the frame it is connected to, and $y(t)$ is the displacement of the frame. The electrical power extracted from this system is the power removed from the system by the electromechanical damping,

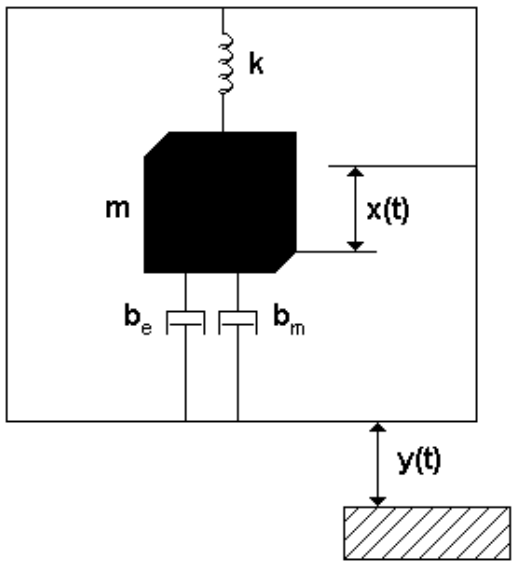

Fig 1. Spring-mass-damper system. Damping consists of two parts, a mechanical that represents losses and an electromechanical that represents power extraction.

$$P=F_e*\frac{dx}{dt} \quad . \tag{2}$$

The differentiated expression becomes

$$P=\int_0^v F_e\,dv \quad , \tag{3}$$

where F_e , the electrical induced force is

$$F_e = b_e * \frac{dx}{dt} \quad . \tag{4}$$

Put into the expression for P and simplified

$$P = \frac{1}{2} b_e \left(\frac{dx}{dt}\right)^2 \quad . \tag{5}$$

Now taking the Laplace transform of (1) results in

$$m s^2 X(s) + (b_e + b_m) s X(s) + kX(s) = -m s^2 Y(s) \quad , \tag{6}$$

$$X(s) = \frac{-m s^2 Y(s)}{m s^2 + (b_e + b_m) s + k} \quad . \tag{7}$$

Furthermore, assuming zero initial conditions

$$Laplace\left(dx \frac{(t)}{dt}\right) = s * Laplace(x(t)) \quad . \tag{8}$$

Define the damping ratios

$$z_e = \frac{b_e}{2\mathrm{m}\,\omega_0} \tag{9}$$

and

$$z_m = \frac{b_m}{2\mathrm{m}\,\omega_0} \quad , \tag{10}$$

where

$$\omega_0 = \sqrt{\frac{k}{m}} \quad . \tag{11}$$

While assuming a sinusoidal input

$$y(t) = Y_0 \cos(\omega t) \tag{12}$$

the expression in (7) now becomes

$$X(j\omega) = \frac{m\omega^2 Y(j\omega)}{-m\omega^2 + (b_e + b_m) j\omega + k} = \frac{\omega^2}{-\omega^2 + 2\mathrm{j}(z_T)\omega\omega_o + \omega_0^2} \quad , \tag{13}$$

where

$$z_T = z_e + z_m \quad . \tag{14}$$

Taking the absolute value and putting into the expression for P it follows that

$$|P| = \frac{1}{2} b_e \frac{\omega^2 \left(\frac{\omega}{\omega_0}\right)^4}{\left(1 - \left(\frac{\omega}{\omega_0}\right)^2\right)^2 + \left(2 z_T \frac{\omega}{\omega_0}\right)^2} \left|Y(j\omega)^2\right| \quad , \tag{15}$$

or

$$|P| = \frac{m z_e \omega_0 \omega^2 \left(\frac{\omega}{\omega_0}\right)^4}{\left(1 - \left(\frac{\omega}{\omega_0}\right)^2\right)^2 + \left(2 z_T \frac{\omega}{\omega_0}\right)^2} \left|Y(j\omega)^2\right| \quad . \tag{16}$$

Here the importance of the system resonant frequency ω_0 becomes apparent. The theoretical maximal output is at this frequency is

$$|P| = \frac{m z_e \omega_0^3}{4 z_T^2} |Y|^2 \quad . \tag{17}$$

Further assume the mechanical damping is negligible

$$b_T = b_e \tag{18}$$

it follows that

$$|P| = \frac{\omega_0^4 m^2}{2 b_e} |Y|^2 \quad . \tag{19}$$

By introducing the quality factor [2]

$$Q = \frac{\sqrt{km}}{b} = \frac{m}{b} \omega \quad , \tag{20}$$

it follows that

$$P_{max} = \frac{1}{2} m \frac{a^2}{\omega} Q \quad . \tag{21}$$

Few assumptions are made to come to this expression. The input motion is assumed sinusoidal and the frequency of the input matches the spring-mass

systems resonant frequency. As for the case of a human body mounted generator this not the case, the movement of different parts of the body is far more random and impulse-like. Therefore, the rest of this section will cover actual measured powers, generator designs and results.

Implementation

The potentially available power to extract from different places of the human body under ideal circumstances is listed in Table 1 [1].

Body heat	2.4-4.8W
Exhalation	0.4W
Blood pressure	0.37W
Finger motion	0.76-2.1mW
Arm motion	60W
Heel strike	67W
Ankle motion	70W
Knee motion	50W
Hip motion	39W
Elbow motion	2.1W
Shoulder motion	2.2W

Table 1. Potential powers available for electrical generation for different kinds of motion and body heat, accordingly to [1].

Those figures are the maximum power extractable. Generators tested for human conditions have showed to give an output less than this. Tests with a piezoelectric actuator utilizing heel strike had an output power in the region 1-2mW, compared to the ideally available power of 67W. Tests with rotary electromechanical actuators could provide approximately 230mW, but only for an uncomfortable long heel strike movement of 3cm. Another example is one 4kg heavy scavenger with a magnet sliding up and down due to human hip moves during walking. This design provided an average of about 0.36W in electrical power.

To further investigate energy harvesting from biomedical devices, figures are needed for the expression (21). In Table 2 is listed values measured on different parts of a human while walking [2].

Location	Acceleration (a) in G's	Frequency (f) in Hz	a^2/f
Ankle	2.5-2.7	1.0-1.7	50-120
Knee	1.7-2.0	1.7-2.0	20-70
Hip	0.4-0.8	1.7-2.0	1-5
Wrist	0.3-0.5	1.0-1.7	1-4
Elbow	0.3-0.5	1.2-2.0	1-2
Shoulder	0.3-0.4	1.7-2.0	1
Chest	0.3-0.4	1.7-2.0	1
Back of head	0.4-0.7	0.8-2.0	1-8

Table 2. Measured values of factors in the expression for possible power output for a motion based scavenger [2].

It can be seen that the human body have locations with relatively high $\frac{a^2}{\omega}$ factors, but instead the quality factor is low. A modest assumption is a Q-factor of 1.

With a proof mass of 1g and assuming a $\frac{a^2}{\omega}$ of 20 and a Q-factor of 1, the theoretical maximal power going into this transducer is of the magnitude $P_{avail,1g} = 0.5 * 0.001 * 20 * 1 = 10\text{mW}$.

Here will follow few examples of generators tested in practical. A rotary prototype was fabricated with a design influenced by the automatic wrist-watch winding mechanism used e.g. by Rolex [2]. The generator consists of a planar coil with an eccentric mass with a number of magnetic pole-pairs turning around the coil, see Fig 2.

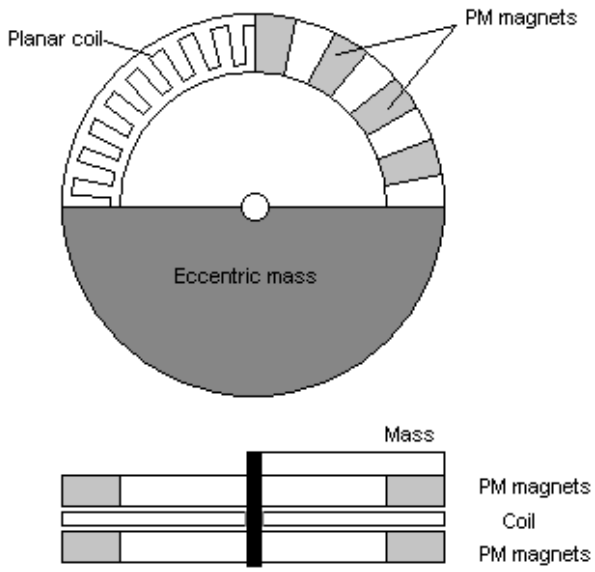

Fig 2. The generator proposed in [2]. An eccentric mass rotates the magnets, causing changes of the magnetic field in the planar coil.

The generator was tested in lab. A varying number of coil layers was used to evaluate influence on performance. The output was then compared to the theoretical value calculated from (21). A 25mm diameter generator was found to have a resonant freq at 2.8Hz and subharmonics at 1.5 and 1.0Hz. During machine generated shaking at these frequencies, and using a resistor with the same resistance as the planar coil for load-match, the generator proved to have an overall efficiency of 5-15% at 1.5Hz and ca 5% at 1Hz. Half of this power is dissipated in the coil due to the matched load. Frequencies 1-1.5Hz is in the typical range of frequencies occurring on a person walking.

However this construction of a generator was not limited to operate at a resonant freq. During real tests while placed on a walking person's knee and ankle it gave an average power output of 3.0 and 3.9μW respectively. The power peaked at 44μW. This output power was dissipated in the load resistor, and it is noted that this needs to be converted to be of any real use. The rms-voltage during these tests was of the order 10-20mV.

In another design, a piezoelectric approach was used [3]. It was noted that the spring-mass system isn't well suited for scavenging due to the low

frequencies present on the human body while moving. Also its resonant dependency is limiting. To come around this, a device with a mass sliding inside a frame, impacting on two piezoelectric cantilevers was proposed. While the frame is subjected to random-like movement the center mass will move back and forth inside the frame and every now and then hit the sides. On the sides, the piezoelectric cantilevers transforms the kinetic energy in the moving mass to electricity.

A mathematical model of the scavenger was made, and it was numerically solved for the output power. The simulation was made for different values of the load resistor and it was concluded that a scavenger with a volume of 1cm^3 and a weight of ca 1g would be able to scavenge 40μW when placed on the wrist of a human, or subjected to a comparable motion.

Another non-resonant dependent generator design has been proposed [4]. A generator with a spherical cavity created by a 3D printer, with copper windings around, it was constructed. Inside the cavity was placed a spherical permanent magnet ball that could move around and rotate freely. Two different ways of windings were tested, and a schematic of these are shown in Fig 3. The motivation behind this design was to pick up motion from all the three degrees of freedom, since the human body does move in all directions. It was also noted that and that a rolling transducer would be more efficient than a sliding one. This design furthermore has the advantage of being able to up-convert the frequency of the input, via the rotation of the ball itself inside will be higher than the rotation of the ball around the space.

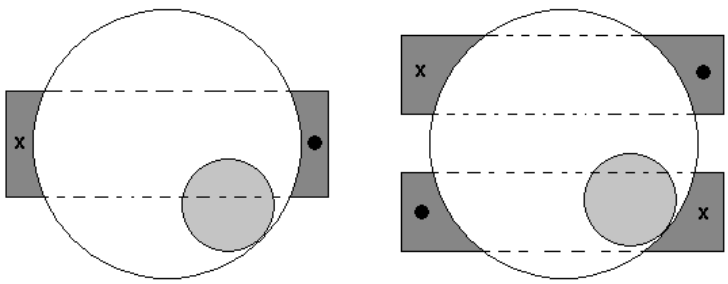

Fig 3. Schematic of two generator designs, only equator winded and offset winded respectively. Magnet ball moving inside. [4]

In order to obtain useful data, the generators were tested on a person either walking or running on a treadmill. Several generators were tested

simultaneously with varying system parameters, coil turns, overall system size and ball-to-cavity diameter ratio. The set of generators were either held in the hand or placed in the pocket. The acceleration of the generators was also measured to get a reference.

In the tests, the open circuit voltage was measured, and a RMS power was calculated assuming a resistive load matched to the coil resistance. By varying the system parameters and plotting the result, the parameters individual importance was noted. The design seamed to have a power density maximum with the offset winded design with 600 turns. Furthermore the power density seamed to increase with the diameters, holding the ball to cavity ratio constant. In the paper cavity diameters between 6.35 and 19.1mm was tested. The ball to cavity ratio gave less clear results, as the power output also depended on the type of motion. While walking mid-sized ratio of 50% was the most efficient, while when running the 70% ball to cavity diameter ratio was better. This was presumed due to the lower amplitude of the motion wile walking better could use the up-converted rotational speed of the ball. However in general, a larger ball is preferred as long as the motion is strong enough to excite the ball into motion.

This design was the most promising one found. Power densities as high as $0.5\mathrm{mWcm}^{-3}$ were measured on a human running with the generator in the person's pocket. The best performing design for walking gave an output of the order $0.1\mathrm{mWcm}^{-3}$ with the scavenger placed in the pocket. If held in the hand this was reduced with roughly a factor 4.

Discussion

Above has some numbers been presented, making it possible to estimate what power levels a motion based scavenger can be expected to deliver. This discussion will be about other parts of a medicinal scavenger.

The lithium battery in a pacemaker can typically store 2Ah, and has an open circuit voltage of ca 2.7V [5]. It furthermore has a typical life expectancy of 5-15 years, which gives the average power consumption

$$P = E/T = \frac{2\mathrm{Ah} * 2.7\mathrm{V}}{5\ years * 8760\mathrm{h}} = 120\mu\mathrm{W} \qquad (22)$$

in worst case. This includes the power consumed by the circuit, the self

dissipated power in the battery and the power leaving the pacemaker as signal to the heart. This value will be used throughout this report as reference.

It can be seen from Table 2 that the power potentially available for scavenging on the human body is of far greater magnitude than required to power most electronics performing digital signal processing. However, this does not guarantee the feasibility of the concept. It will eventually depend on how good the actuator is on transforming the kinetic power into electrical power. From the tested designs it is clear that there is a large gap between these numbers. This could suggest that the generators are poor designs, but that is not likely for several reasons. Mainly because several teams independent of each other has come up with designs that performs similar. They also use different ideas, and their design covers the established design principles. It rather seams that a scavenger placed outside the body can't come close to the actual mechanical work carried out by the muscles.

The generators described above are built and tested on actual human conditions. The placement of the scavenger proved to have large effect on the outcome. For implants placed in the chest area or head, the available power from the motion is less than around the hips due to the body absorption ability. At best, the scavenger should be able to power the implant, with a battery as buffer, indefinitely. The numbers presented above imply that a scavenger at least could extend battery lifetime, depending on size restrictions. If the scavenger can be implemented and reliably integrated with the implant it could decrease patient discomfort and risk vastly by reducing the number of operations and hospital visits, especially since scavengers typically should be used where battery replacement is very difficult.

However there is some uncertainty with this novel concept. Having a ball moving around inside ones chest or head could affect patient discomfort. The additional mechanics in the implant furthermore increases system complexity and hence its failure rate. Before an implant can use this, a safe concept needs to be proposed, fulfilling all requirements for medicinal electronics.

A different approach is to place the scavenger on a place where it can be easily replaced, like outside the body. It could be in the form of a wrist watch like device, or some other similar design placed comfortably outside

of the body. The scavenged power then needs to be transferred into the implant. This could be done through induction, where a transformer is built with the primary winding outside the body and the secondary winding inside, coupled to the implant. The scavenger could collect energy for a while before transferring it to the implant. By transferring a larger amount of power instead of the lower one available for scavenging, the implant itself does not have to deal with the difficulties associated with low power and voltage levels. The implant can then in principle be left as it is with the scavenged energy transferred passively to it. More about this will follow in the next chapters.

As already mentioned, different people behave differently. This has to be taken into consideration when deciding on a scavenger system and an individual adapted solution should be tested out. If not enough motion is available, perhaps different sources of energy are. More about those sources follows below.

Radio frequency signals

Harnessing the energy in radio signals is another way to scavenge for energy. The use of wireless communication is increasing, and so is the power content in the ether from these signals. This part will investigate whether extracting this power is a feasible way to power electronics.

Focus is put at scavenging for higher frequencies and for frequencies where high power densities can be expected. At higher frequencies the waves are small enough to allow for antenna sizes usable for human implants. The GSM standard starts at 900MHz, which corresponds to the wavelength $\lambda \approx 0.3\text{m}$. That is small enough to make antennas applicable for implants, and power can be expected to be found here due to telecommunication traffic. Hence, this frequency is set as lower limit.

The section will start with analyzing what radio frequency, RF, power levels to be expected in different environments, to get an idea of the signal and power levels available for scavenging. Also an environment with a wireless network will be investigated with respect to its radiated power, after that will follow a few descriptions of different antennas designed with the purpose to scavenge for RF energy. Last comes a discussion about the usefulness of harvesting for RF energy in a human body.

RF levels in Europe

To find out what power levels exists from radio frequencies, measurements of real ambient RF levels in Europe has been made [6]. The question is whether or not the ambient RF energy from the GSM-900 and GSM-1800 is enough to power small wireless sensor systems. RF energy here refers to RF energy available through public telecommunication systems, which are not introduced with the purpose of transferring power. To answer this question, data was gathered to asses the power densities in different environments in Europe.

All the data in the study comes from the COST Action 244bis: “Biomedical Effects of Electromagnetic Fields”. The COST is a European initiative to investigate the “Potential Health Implications from Mobile Communication Systems”, going under the name COST-281. COST is a framework for

international research and development cooperation. Quoted from the website http://www.cost281.org: “The main objective of the Action is to obtain a better understanding of possible health impacts of emerging technologies, especially related to communication and information technologies that may result in exposure to electromagnetic fields”. 25 European countries actively participate in this action (2010).

From the data in the COST action, the corresponding power densities were derived. These power densities varied a lot depending on the surroundings. Difference was made between eg inner city/outer country and industrial areas as well as measurements close to the ground and up on a roof. Even the distinction between indoor at different distances from the closest window was made. Only the main results are reviewed here. With the largest variations - being close to the ground - removed from the data, it can be summarized that expected power densities in the GSM-900 band, a distance of 25m to 100m from closest base station, is in the region of $0.1\text{mW}/m^2$ to $1.0\text{mW}/m^2$. These power were the peak power density for a single frequency spot-measurements with no regard to the amount of traffic, ie as “normal” conditions as possible. For the band as whole, the density can be expected to be a factor 3 higher for the same conditions due to multiple bands are in use at the same time carrying different calls. Measurements on the GSM-1800 band indicated that for the time of the study (-96 to -00), this band can be expected to have similar power densities.

Next, measurements of the radiation from a WLAN router was made [6]. A router typically transmits far less power than a GSM base station, but is on the other side intended for close range use. The authors themselves carried out measurements in their office building with a dipole antenna in three orthogonal directions. Each measurement lasted for half an hour during a normal working day. The antenna was placed 7-8m from the router (different sessions) and the result was normalized to get the power density. The amount of traffic is not known, but is said to be “extremely low”, again with focus on a normal situation in an office building. The average power densities obtained was of the magnitude $1\mu\text{W}/m^2$ at 7m from the transmitting antenna, in a relatively open area in the office.

The radiation from a WLAN environment is therefore regarded as not feasible for energy scavenging, since it's of too low magnitude. The radiation from the GSM bands is of a higher magnitude, but requires

relatively large antennas to harvest a usable amount of energy.

Implementation

To efficiently harness stray RF power in the 2-18GHz region, multifrequency broadband rectennas with dual circularly polarized rectenna arrays has been proposed [7]. A rectenna is the combination of an antenna receiving the RF energy and a rectifier converting the signal to direct current, DC.

One design was manufactured, and was measured to give up to few hundreds millivotls for most of the intended frequencies, at input power in the range $1\mu W/cm^2$ to $10mW/cm^2$. Furthermore the design had a demonstrated efficiency in the magnitude of 20%. The design simply uses a source-pull Schottky diode as rectifier.

The rectified power needs to be processed. The processing circuit needs to be as efficient as possible, hence it is important to keep the parasite leakages to a very low level. This is of specific high importance when constructing DC-DC converters for very low powers, since the parasitic capacitance is a strong limiter of the efficiency. A process called FD-SOI (fully-depleted silicon-on-insulator), has been showed to have as little as 1/1000 parasitic capacitance compared to traditional CMOS technique. Using this technique, a custom power converter with a two-stage switched capacitor (SC) converter, and an associated MPPT circuit for optimal loading of the rectenna was implemented [7]. The SC stage uses on-chip buffers, and can generate eight distinct input/output voltage ratios in the range 1/3 to 3. These ratios are externally controlled. The controller itself adjust switching frequency to adapt to the voltage building up in the storage capacitor; a higher frequency for higher built up voltage. With a fixed input power of 10μW, the converter was found to have an efficiency above 60% for most output voltages. However this require actively changing of switching topology to maintain, as each topology proved to has a quite narrow band of high efficiency.

The 2.4GHZ band is especially interesting for power harvesting, since a lot of RF sources exists there. 802.11 has a standard there for WLAN, a very common wireless network access in offices, Bluetooth operates in the 2.4GHz band, some cordless phones and microwaves radiates in this band. Many countries, including Sweden, also have this band free of license. This

means anyone can transmit general information in the band, with a limitation on the output power. In Sweden this level is set to 25mW, or 14dBm, accordingly to the Swedish “Post- och telestyrelsen” [8]. The highest transmitted power allowed in this band for network communication is 100mW or 20dBm. The Bluetooth standard has 3 classes with a transmitted power at respectively class A: 0dBm, class B: 4dBm and class C: 20dBm. The transmitted power for 802.11 devices varies, but is usually 10-20dBm.

Consider the case of deployment of a wireless sensor network in an office space, scavenging for RF energy from the ambient power levels plausible in a corporate office [9]. The 2.4GHz band is chosen due to its commercial popularity.

The path loss is described by the Friis transmission equation (in dB)

$$P_L = 20\log(4\pi d/\lambda) \quad , \tag{23}$$

where d is the path distance, and λ is the wavelength. At an average of 2.45GHz, $\lambda = 0.122$.

However, this only applies to a free space. For an indoor environment the model needs to be adjusted, and in general [9]

$$P_L = P_L(d_0) + 10\mathrm{n} * \log(d/d_0) + X_\sigma \quad . \tag{24}$$

P_L is the total path loss from the transmitter to the receiver, $P_L(d_0)$ is the path loss at a reference point close to transmitter, n is the path loss exponent typically in the range 3-5. X_σ is a random variable with standard deviation σ to catch the unknown state of obstacles, people moving around and multipath propagation, etc. The total received power will be the sum of the transmitted power, the gain of the transmitting antenna and the receiving antenna, minus the path loss.

As for the circuit design directly after the antenna, simulations has shown an interesting thing. The standard choice is thought to be using a rectifying diode in series with the source, like in Fig 4b. But simulations has found that it can be more efficient to put the diode parallel with the source, shorting out the negative contribution of the AC-source the antenna (a likely error was made here in the original article, where they flipped direction on the diode) accordingly to Fig 4a [9].

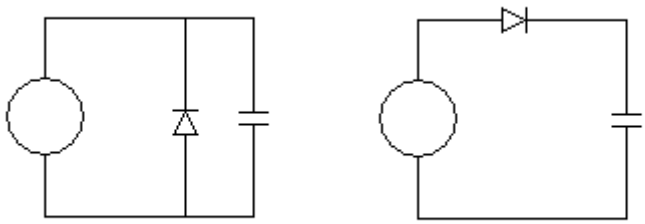

Fig 4. Two different layouts. a) with diode in parallel b) with diode in series.

The smoothing capacitor will then only see the positive half-wave of the source, and its output will average to an output higher than that of the standard series-diode design.

One difficulty in harvesting the energy from very small signals, like these, is that a large part will never get passed passive components like a diode. To overcome this, only components intended for small signals and high frequencies should be used. As an example, the Schottky diode Agilent HSMS-2850, which is a zero bias detector diode developed for small signal at high frequencies, can be mentioned. It has a very low forward voltage drop of 0.15V at 0.1mA.

Heavy constraints are often put on the size of the total sensor node at design level. The planar folded patch antenna, which can be manufactured in a chip-sized design, is a possible choice. This design also have the benefits of ease of manufacturing and low cost [9]. The principle design of the antenna is shown in Fig 5. Here follows a description of a tested design. The width of the top patch is 7.5mm and the total height is 5.5mm. The thicker feeding via is drawn through the ground plane and is connected directly to the Schottky diode. The whole design is embedded in a high resistivity polycrystalline silicon (HRPS) substrate with a high dielectric constant $\varepsilon = 11.7$ to further decrease the size. This size is $\lambda/16$, compared to the normal 62mm $\lambda/2$ antenna. The

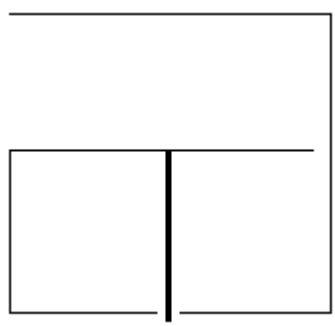

Fig 5. Folded patch antenna.

cylindrical feeding via has a radius of 100µm. Noticeable is that the resonant frequency can be varied, and thereby fine tuned, by varying the height of the antenna. The goal was to construct an antenna that optimizes the harvesting in the 2.41-2.47GHz band.

In a design with multiple antennas put in a 4*4 series-array, an output voltage of 0.7V was obtained at an input power of -25dBm (power density*antenna area).

Discussion

The power content in radio frequencies has proven to be in the range low $\mu W/m^2$ to low mW/m^2 . There are though rectennas with good overall efficiency, capable to harvest energy from these levels.

A major fact to consider for scavengers for human implants, is the damping of the tissue surrounding the implant. The skin and the lower layer will damp and reflect parts of the RF power. In a LAB View based model of the human skin, fat, bone and muscle layers was concluded that the total reflected power from the skin at is 45% at 900MHz, and 64% at 1800MHz [10]. The reflections of the underlying layers are lower. The different layers of tissue also dampen the signal. How much is best described by the penetration depth, defined as the distance from the surface where the power has dropped to $1/e \approx 0.37$ times the level at the surface. The penetration depth for muscle tissue, which is similar to skin [11], is 35mm for 900MHz and 22mm for 1800MHz [12]. Furthermore, the penetration depth for 2.4GHz is in the region 13-26mm [11]. This has to be accounted for if a scavenging implant is to be placed deep.

Light

Scavenging for light energy is perhaps the preliminary way one would think of. At these days of increasing environmental awareness, solar cells are fast gaining popularity. This section will cover the area of scavenging for light energy for medical applications. It is organized in the following way. First, the overall efficiency for different technologies available today will be presented. This should be kept in mind for the discussion found last in this section about what power levels are available at what places. Secondly a brief explanation about the optimal loading of a solar cell will follow. After that follows a description of a scavenger where a solar panel is used as energy input, and lastly comes a discussion.

Efficiency

A lot of work is being put at increasing solar cells efficiency [13]. News about record breaking solar cells keeps coming on a regular basis. From the history of development it can be seen that that solar cell efficiency has evolved. The chart from the “National Renewable Energy Laboratory, NREL” below shows how the class-leading “champion cell” efficiency for different semiconductor materials has increased over the last decades.

The graphs shows the results obtained in a laboratory environment, reaching numbers that the manufacturers don't expect high volume production panels will reach. But the increasingly results in lab seams to translate into a better performance at the commercial cells, first Solar reported their commercial panel efficiency to grow from 10.9% to 11.2% from 2009 to 2010.

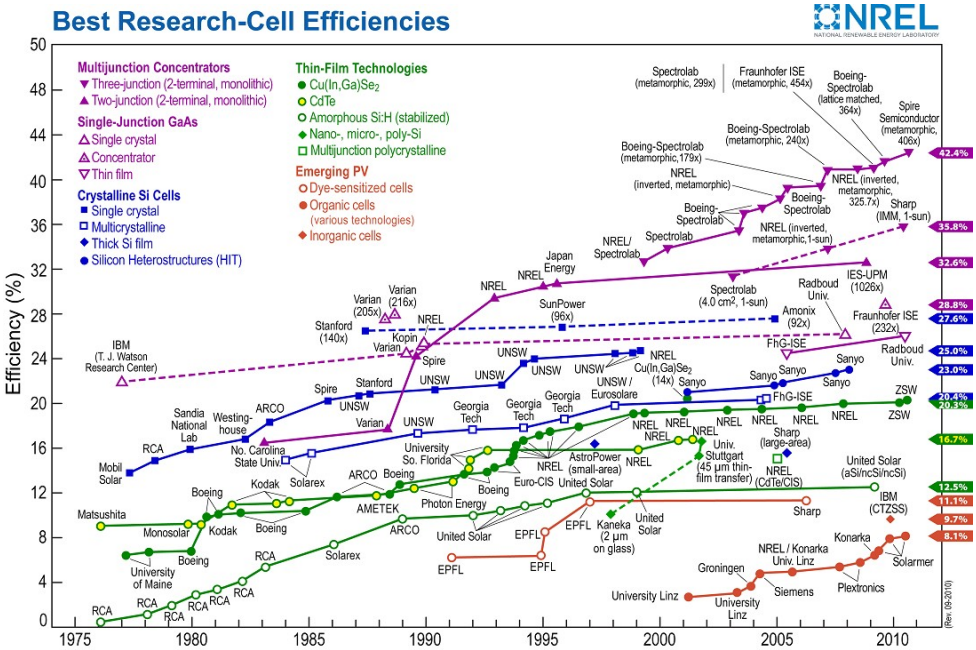

Fig 6. Development of the class leading solar cell for each technology. Figures for best result obtained in laboratory, not commercial available. Data compiled by Lawrence Kazmerski, National, Renewable Energy Laboratory (NREL). Image is in the public domain.

The current class leading efficiencies is presented in table 3 below.

Material	In laboratory	Commercial panel
Crystalline Si	25%	19.3%
CIGS	19.6%	11.2%
Cadmium-telluride	N/A	11.3%
Amorphous Si	11.9%	9.2%
Multijunction concentrator	41.3%	N/A

Table 3. Best efficiencies in laboratory and for commercial solar cells respectively using different technologies.

Interesting to note is that the laboratory efficiency of silicon based solar cells start to come close to the theoretical limit of ca 29%. A contributing factor to this development was the (a bit unexpected factor of) world shortage of silicon in 2005 till 2008. This increased the price of silicon to almost a tenfold its normal prices, pushing the manufacturers to make their

panels more efficient to make more money on each kg of silicon. But today, after the price on silicon has fallen back to normal levels, boosting the efficiency is still a commercial reason. Reducing the amount of silicon in a panel could yield higher profit.

CIGS, copper-indium-gallium-diselenide, is the thin-film solar cell with the highest proved efficiency, with several companies laying close to each other in the competition of efficiency. Amorphous cells typically have a lower efficiency, but are cheap to produce thanks to its low silicon content. The amorphous cells also have shown good efficiencies at dim light levels. Cadmium-telluride is the material First Solar use in their record breaking cost effective cells, with below 80cents per Watt of peak power in manufacturing cost. These are claimed to have an average efficiency of 11.3%. With a production capacity of 1.4GW in 2010 First Solar is the world's largest manufacturer of solar panels [14].

Cells with a multijunction concentrator are the cells reaching the by-far highest efficiencies. However, they are only functional in a laboratory environment with light intensities several hundreds times higher than that of the sun. These kinds of cells are therefore complex to install commercially, demanding the use of mirrors and lenses.

MPPT

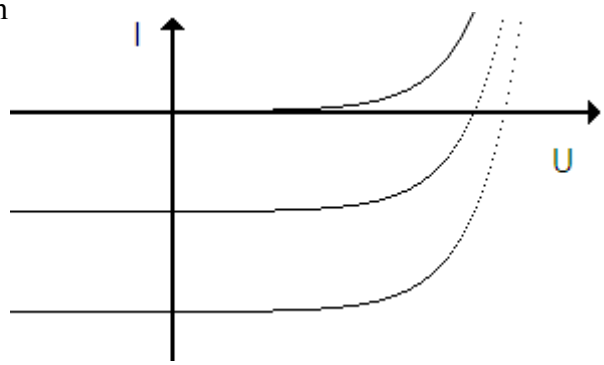

Fig 7. Current-voltage curves for a solar cell under discrete different lightning conditions.

When extracting power from any source it's of fundamental importance to do so at an optimal loading point, or else available power will be left unexploited. A method to find this point is to do a maximum power point tracking (MPPT). If the power source is an ideal voltage source with an internal series resistance (assumed constant), then optimal loading is done when the source is loaded with a resistance equal to the internal resistance. A solar cell however, is not a voltage source with a series resistance, but

rather a diode. The U-I characteristics will thus be exponential and not linear. Therefore the MPPT is best illustrated in the following way. In Fig 7 is shown current (I) – voltage (U) curves for a solar cell at different lightning condition [15]. The topmost curve is at complete darkness, and at higher light intensities the short circuit current (at U = 0) will increase (roughly) proportional to the intensity. To get the most power possibly out from the cell the factor

$$P = U * I \tag{25}$$

should be maximized. This corresponds to choosing the point on the current curve that maximizes the area from the working point to the axis.

Implementation

This section will be about a solar power based scavenger [16]. An inductor-less MPPT design was chosen due to size restrictions. The system consists of a photovoltaic cell, a DC/DC converter and a storage battery. Solar power was chosen as energy source because light energy is the most popular energy form to scavenge for because of its availability and power density. Also the area has been vastly exploited, which makes the technology mature and a lot of material is available on the subject. A DC/DC boost converter is required in order to perform an MPPT when the photovoltaic voltage is less than the battery's. An inductor-less design was chosen due to size restrictions. Focus was put in boosting the voltage at low light conditions efficient. The switching frequency was tracked to its optimum by the generic hill climbing method, which means that the switching frequency was altered until the highest output was obtained.

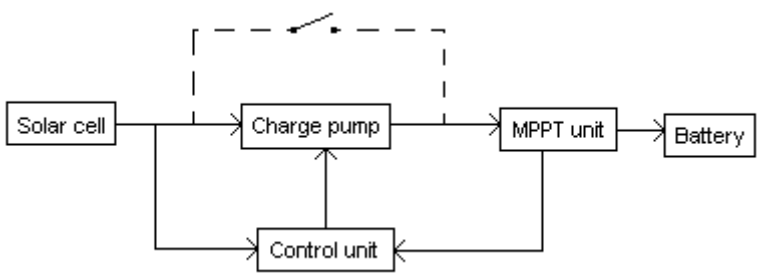

Fig 8. Block diagram for the proposed MPPT design. The Charge pump is bypassed at high solar cell voltage. The control unit will alter the switching frequency until the highest output is obtained.

The system consists of a voltage booster that is bypassed by a switch at high light conditions, the MPPT block - with its associated Power Point tracker - and a 125mAh li-ion battery. The control circuit is powered by the battery, and the scavengers output connects to the poles of the battery. Since the battery clamps the voltage from the photovoltaic cell or the boost converter, maximizing the system power means maximizing the current going into the battery. The sensor circuit is a discrete OP-like stage with a current sensor resistor $R_S = 300\text{k}$. The voltage read over this resistor is then sampled in two capacitors, alternating which one. This makes it possible to tell whether the current increases or not. Based on this the circuit generates a control signal to tune the switching frequency. This whole sample and optimizing is done only with a certain time period in order to reserve on energy. When sensing current in R_S , it will dissipate part of the power that could go to charging the battery.

The MPP tracker was fabricated in 0.35µm CMOS, and two 6*6cm mono-crystalline solar cells was used as power source. The MPPT was tested with very good result. For a number of fix illuminations (370-1700lux), the MPPT was disabled and the switching frequency was tuned by hand to find the optimal power point. Then the power tracker was enabled and did the same job. The result is summarized in table 4 below.

Illuminance (lux)	Ideal system (µW)	System with MPPT (µW)
368	105	101
706	333	327
1141	533	529
1734	779	776

Table 4. Data for the MPPT in [16]. The system shows good performance compared to the optimal loading. Illuminance levels ranging from a normal office light to a bit above the level expected in a TV studio.

The result shows that it is possible to construct a MPPT with high efficiency with 100µW input power.

Discussion

Accordingly to "World Radiation Center, Physikalisch-Meteorologisches Observatorium Davos", the total sunlight power density on the top of the earths atmosphere is $1360\,W/m^2$ [17]. How much of this will penetrate down to the ground will depend on damping in the atmosphere, angle of view and time-of-day. This has to be considered when planning a sunlight scavenger system, in order to predict the possible outcome. Measurements should be done to ensure enough ambient energy to scavenge for the proposed system. If the scavenger system is to be used for a medical implant, the damping of the skin also has to be considered. The penetration depth for the human skin in the visible light spectrum is about 1mm [18], meaning that roughly e^{-n} percent of the intensity at the surface will remain at a depth of n mm.

The majority of solar cells are rigid and does not bend. This makes it unpractical to place a solar based scavenger close to the skin. However, since implants today are rigid too, placing a layer of solar cells outside the implant could be possible. That would though require the coating of a clear layer of the solar cell that does not react with the body fluids. The normally used outer layer of titanium today shows good ability to resist body fluids, but it does not let through light very well.

It can be worth mention that there is a team at Stanford University who has developed a stretchable solar cell. Professor Zhenen Bao claims that the solar cell can be stretched 30% in two directions without loss of functionality. The cell is in fact intended for use on an artificial skin. That could open up for the possibility of embedding solar cells with human skin.

The relatively high absorption of light in human skin seams to suggest that solar cells are hard to integrate directly with implants. That is despite the power density from sunlight itself is quite high. It is integrating the scavenger with an implant that will cause losses. A way to go could be to place the scavenger outside the body, perhaps through the use of special clothing, or a wrist watch-like device with a solar panel in its outside. This outer device then needs a way to transfer its collected energy in to the implant. The most attractive solution for this is to do it through induction, since that requires no galvanic contact. A coil or rectenna is then placed not too deep under the skin. The penetration depth for radio frequency signals is significant larger than for light, in the order of 35mm for 600MHz [12]. For frequencies often used for RFID energy transfer (13MHz) the penetration

depth is even longer. A wrist watch-like unit placed on the arm should be designed to re-reflect the reflected RF energy from the skin. It could furthermore be designed with the intention of having double purpose. Through regular checks at a clinic, the implant could use the scavenger to "fast charge". When the patient is between checks, the scavenger would extend these intervals. Thus has a decreased patient discomfort been achieved. The scavenger could even be optional.

The actual amount of energy available to scavenge will depend on outer factors. How much time the patient spend outdoors will have large significance. Accordingly to the Swedish authority in charge of working environment, Arbetsmiljöverket, the recommended illumination level at an office is 500lux. This is appropriately 0.5% of the illumination in direct sunlight [19], and the power density drop with the same factor.

An example. Assume that the maximum comfortable area of an outer scavenger is 10cm^2 . In direct sunlight the scavenger could then itself collect something like

$$P_{store} = \eta * P_{in} = 0.2 * 1\text{W} = 0.2\text{W} = 200\text{mW} \quad , \tag{26}$$

which is by far more than the required 120μW the pacemaker consumes. Even at a moderate efficiency of 10% for the following inductive transfer, 20mW remains. Assuming a little over one hour spent in the sun every day, the scavenger will (moderately estimated) average around 1mW. That is approximate a factor 10 more than needed to power the pacemaker.

The area of scavenging for energy in light will be covered in further detail in section II of this work, where an experimental photovoltaic based scavenger will be designed.

Thermal gradients

In this section, energy harvesting from temperature gradients will be covered. Power from thermal gradients is obtained by using thermoelectric generators, TEGs. A TEG converts a temperature difference to a voltage, and this voltage generates power when loaded. Temperature gradients are available on the human body, as its temperature often is higher than that of the surrounding. Whether this method is usable for scavenging or not will be explored in this section, which is organized as follows.

First a mathematical model of a TEG will be presented. This will explain the relation between basic parameters of the TEG, after that follow a few examples where utilizing thermal gradients for energy conversion is implemented. Last in the section the results will be discussed with respect to the method's usefulness for use in medical applications.

Modeling

Here the characteristics of a TEG will be modeled [20]. This aims at giving an understanding of the ingoing parameters, and to end up with an expression for the maximum power from the TEG when used as generator. This analysis will also lie as basis when approximating the TEG efficiency later.

Consider Fig 9 below.

The TEG is made of a p- and a n-type semiconductor joined at the hot junction. Outside of these are electrically isolating and thermally conducting ceramic plates mounted. The semiconductors have a Seebeck coefficient α_p (positive) and α_n (negative) respectively, making the overall Seebeck coefficient

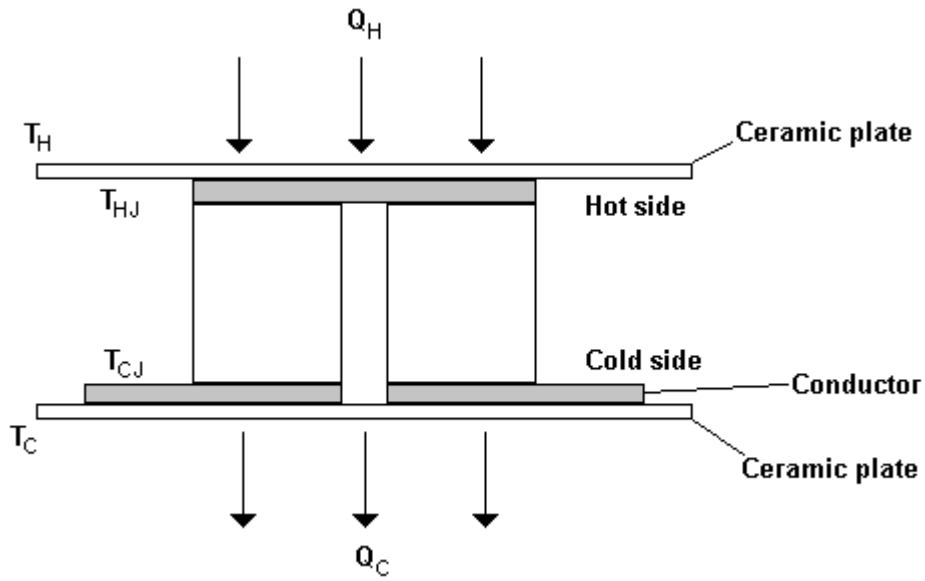

Fig 9. Model of a TEG. A p- and a n-type semiconductor sandwiched between two layers of ceramic plates.

$$\alpha_{pn} = \alpha_p - \alpha_n \tag{27}$$

positive. Furthermore the Seebeck coefficient is assumed temperature invariant. This assumption is not entirely correct, but its effect is typical insignificant.

The rate of heat (unit: power) exchanged at any junction due to the Peltier effect is

$$Q_X = \alpha_{pn} T_X I \quad , \tag{28}$$

where T_X is the absolute temperature of that junction, and I the current in the junction loop. Assume that I flows from the hot to the cold side in the p-type conductor, then a positive Q_H means heat flowing in, and a positive Q_C means heat flowing out.

The direction of the heat flow is constant, see Fig 9. A (supposed waste) heat source heats the hot-side ceramic plates outer side to T_H . The inside of that plate has the temperature T_{HJ} . The heat is then transferred trough the conductors to the cold plate's inner and outer side, T_{CJ} and T_C respectively and then out to an outer environment.

If a load resistance R_L is connected to the TEG a current

$$I_L = \frac{V_G}{R_{in} + R_L} = \alpha_{pn} \frac{T_{HJ} - T_{CJ}}{R_{in} + R_L} \tag{29}$$

flows, where

$$V_G = \alpha_{pn}(T_{HJ} - T_{CJ}) \tag{30}$$

is the voltage due to the Peltier effect proportional to the temperature difference between the junctions.

In the following it is assumed that the thermal conductance of the ceramic plates is large enough to be negligible,

$$\Delta T_{TEG} = T_H - T_C \quad . \tag{31}$$

With the TEG having an internal series resistance of R_{in} , the power in the load R_L can be written

$$P_L = I_L V_L = I_L(\alpha_{pn} \Delta T_{TEG} - I_L R_{in}) \quad = \tag{32}$$

$$I_L \alpha_{pn} \Delta T_{TEG} - I_L^2 R_{in} \quad . \tag{33}$$

Substitute I_L from (29),

$$P_L = \frac{(\alpha_{pn} \Delta T_{TEG})^2}{R_{in} + R_L} - R_{in} \frac{(\alpha_{pn} \Delta T_{TEG})^2}{(R_{in} + R_L)^2} \quad = \tag{34}$$

$$\alpha_{pn}^2 \Delta T_{TEG}^2 \frac{R_L}{(R_{in} + R_L)^2} \quad . \tag{35}$$

Optimal load conditions will be when then load resistor equal the internal resistance, and the maximum power extractable is

$$P_{L,max} = \frac{\alpha_{pn}^2 \Delta T_{TEG}^2}{4R_{in}} \quad . \tag{36}$$

The Peltier cooling effect on the hot side will lower the possible output, but will typically be negligible.

To get an estimation of the efficiency, consider the rate of total heat exchanged at the both sides. It is the sum of the Peltier effect, the thermal conduction through the element accordingly to Fourier's law and the heat loss due to the current flow through the internal resistance

$$Q_H = \alpha_{pn} T_{HJ} I_L + K_{in}(T_{HJ} - T_{CJ}) - 0.5 I_L^2 R_{in} \quad , \tag{37}$$

$$Q_C = \alpha_{pn} T_{CJ} I_L + K_{in}(T_{HJ} - T_{CJ}) + 0.5 I_L^2 R_{in} \quad . \tag{38}$$

The major term will be the thermal conduction. The value of K_{in} should be found in the data sheet of a TEG. As seen the input power is proportional to the temperature difference, while the output power is proportional to the squared temperature difference. This makes the overall efficiency approximately proportional to ΔT_{TEG}, and should be on the form

$$\eta = k * \Delta T_{TEG} \tag{39}$$

where k is a constant.

Implementation

In order to provide a figure of merit for commercial TEGs, an experimental setup with several commercial TEGs is reviewed here [20]. The TEGs were tested in a setup sandwiched between two auxiliary thermoelectric modules, and their surface temperature was measured. This setup allowed for keeping both the temperature difference and mean temperature at desired levels. The open circuit voltage was measured, and so was the output power for different resistive loads. This found the model of the TEG as a variable ideal voltage source with a series resistance to be accurate. Furthermore the output voltage was very linear with the applied temperature difference, as expected from the theory.

It can be noted from these tests, that the form of the expression for the efficiency

$$\eta = k * \Delta T_{TEG} \tag{40}$$

proved to consist with the test results. Using data from [20] listed in Table 5 for

$$\Delta T_{TEG} = 10 \quad , \tag{41}$$

the efficiency at load-matched conditions can be calculated as

$$\eta = \frac{P_{out}}{P_{in}} = \frac{\left(\frac{V_g^2}{4 * R_{in}}\right)}{K * \Delta T} \quad , \tag{42}$$

and Table 5 can be extended with the corresponding values of k:

	K [W/K]	R_{in} [ohm]	V_g For $\Delta T = 10$	k
TEG1	0.67	7.6	0.9	$0.40 * 10^{-3}$
TEG2	0.50	2.1	0.4	$0.38 * 10^{-3}$
TEG3	0.18	6.8	0.5	$0.51 * 10^{-3}$

Table 5. Test data for three TEGs to evaluate their efficiency. The TEGs are the following. TEG1: Supercool PE-127-14-15, TEG2: Kryotherm TGM 127-1.0-2.5, TEG3: TGM 254-1.0-1.3.

Another useful figure is the so called Power Factor, PF. The PF is defined as the highest power output at matched-load conditions per module area and squared temperature difference, and hence has the unit $\mu W m m^{-2} K^{-2}$.

The squared temperature difference is because convenience due to the maximum power is proportional to the squared temperature difference. For the tested TEGs the magnitude of the power factor is in the region $0.1 \mu \mathrm{Wmm}^{-2} K^{-2}$ to $0.8 \mu W m m^{-2} K^{-2}$.

Last was made a test, where a wireless sensor node was powered by one of the TEGs. The node circuit consisted of a TPS60303 charge pump, which start to work when the voltage from the TEG exceeds 0.9V, and then delivers a stable 3.0V output. To wireless transmit the information, a MAX1472 RF transmitter was used. This system was concluded to work properly when the temperature difference on the sides of the TEG exceeded 34K.

The somewhat large required temperature difference is partially explained by the fact that the charge pump does not start until the TEG voltage exceeds 0.9V. Enough power is available at less ΔT_{TEG} , but collecting power at such low voltage requires additional circuitry. A better voltage-matched TEG would likely perform better.

To make a working thermal energy scavenger for the human body, the body's thermal conditions has to be considered at design level [21]. The problem of scavenging for power from human body heat is mainly two things. Firstly, the body temperature rarely is more than 10-15K above ambient air, and for the second, only a small fraction of this temperature difference will drop across the TEG. This is due to the TEGs low thermal

resistance compared to the ones for the human body and ambient air. This is thus a non load-matched conditions kind of problem. In the design of a scavenger, a specific shaping of the die was used, and a heat sink was introduced, in order to make as much of the temperature difference as possible to drop across the generator. The thermocouple (a p- and a n-type poly-SiGe) itself has a trench etched, to be better thermally separated from the die, in order to increase its thermal resistance. Additionally to this, the substrates were laid as a step, in order to increase their length and hence its thermal resistance. Furthermore the width of the thermocouple at the step is made narrower than the contact surfaces, to further increase the thermal resistance and to get a low contact resistance.

The design was analyzed using FEM software and the thermal resistance of a single thermocouple was calculated to $1.28*10^5 K/W$. The total TEG consisting of 4200 thermocouples has a thermal resistance of 30K/W. This is still too low compared with that of the body and air that sum up to about 1000K/W.

Additionally to this, the thermopile was mounted on a Si substrate rim. This has several advantages. The surrounding Si will be replaced with less thermal conducting air. Moreover the Si "in series" with the thermopile is more conducting than the thermopile, which leads to most of the temperature gradient will be across the thermopile. On top of this an additional heat sink was mounted on the thermopile.

The output from the design with 4200 thermocouples was calculated, assuming a constant temperature difference of 14K. A temperature difference across the thermopile of a few K was obtained, with the length of the thermocouple legs being a handful microns. The output performance of a watch-sized scavenger was found to be 1-2µW, and an output voltage of about 1V was obtained.

The thermopile was fabricated and tested, before etching the trench and before placed on the rim. Testing conditions were only a small fraction of 1K, and the performance was found to be $13 mVK^{-1}cm^{-2}$ with natural convection, and up to $53\text{mV}\,K^{-1}cm^{-2}$ under forced convection. A larger output voltage was expected upon process completion.

So far, thermal gradients in space has been used as power source. Another approach is to use thermal variations in time, rather than space [22].

Pyroelectricity is the material property to convert a temperature variation to

electricity. This works much like piezoelectricity - and in fact often piezoelectric material also have pyroelectric properties - with temperature exchanged with displacement. Pyroelectricity is mostly dependent of the rate of temperature variation, and measurements with a 10K increase over 20s has showed a power density of ca $1\mu W\,cm^{-2}$ for common pyroelectric materials [22].

Another idea is to use magnetic material, since the magnetization of a material often is dependent of temperature. When the temperature of the magnetic material changes, the magnetic flux changes too, which could be used to generate power. An evolution of that idea is to use the flux changes close to the Curie point, where the flux changes are large even at small temperature differences. The Curie point is the temperature where a magnetic material loses it magnetization. The effect is reversible, the material regain its magnetization after cooling down. It was from this the idea of a prototype emerged [22].

The prototype, showed here in Fig 10, is composed of the following parts. A piezoelectric beam is fixed at one end. The beam is made up of two piezoelectric materials around a central sheet of metal. At the other end of the beam is attached a NdFeB magnet. This magnet will swing in the field between two ferromagnets, which have a tunable Curie point fixed at ca $T_C = 45\,^{\circ}C$. The working principle is as follows. The beam is at equilibrium between the two FeNi compounds when temperature is over T_C , which means the FeNi compounds have a relative permeability of 1. When the temperature decreases below T_C , magnetic forces will start to act on the magnet. Below some threshold temperature the magnetic forces will be large enough to attract the magnet to one of the FeNi compounds. Due to the magnetic forces depending more than linear on the distance the magnet will make a "jump". While moving the bending piezoelectric beam will generate a

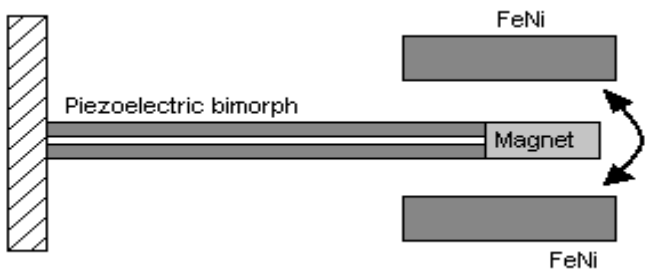

Fig 10. Operating principle for the prototype. The magnet is either attached to one of the magnets or oscillating between them.

voltage. When the temperature increase above some threshold temperature, the spring force from the beam will be greater than the magnetic force holding the beam at its end position, and the beam will spring back to its equilibrium. This movement of the beam will also generate a voltage.

The tuning of design parameters was carried out numerically in Matlab/Simulink. Simulations then showed the principle to work as intended, in a model with a beam swing of $\pm 0.85\text{cm}$ and temperature varying only $1^{\circ}C$.

No figures exists that reveal this methods feasibility, the design rather shows that there are a few concepts out there that still can be tried.

Discussion

This section has made a model of a thermoelectric generator, and investigated some of the most promising designs. The one with thermocouples is the one that seams most promising, with design intended for use on human and giving relatively high output voltage. A well chosen output voltage will make it easier for the electronics driven by the scavenger to make use of it. Magnitudes of a few volts were mentioned in the 14K temperature difference test, which may be a bit large to be realistic when the scavenger is placed on a human. The body's temperature regulating will cause less reheating of the area cooled by the TEG.

From the articles available on the subject, it seams presumed that the earlier proposed system with placing the scavenger outside the body in a wrist watch-like design is to be used. This is natural, since it is here that largest temperature difference caused by the body is found. Placing a thermoelectric generator inside the body in a constant temperature environment will have no effect. The scavenger could be constructed with multiple functionality. A suggestion is to combine body heat and light as energy sources, in the form of a thermopile with a silicon heat sink on the outside consisting of solar cells. Perhaps the two methods combined would provide a usable amount of energy, when one is not available perhaps the other is. More sources of energy could be combined in the scavenger, in a try to assure that at least one form will generate power.

Driver electronics

In basically all applications, the power being scavenged must be transformed to fit the specifications of the main power consuming device. The varying nature of the scavenged power also implies the need of some form of active power optimum tracking to load the generator at the most efficient rate. Depending on the nature of the energy, this will be more or less hard to do in real time. A vastly varying source or a source of stochastic nature will need a continuous tracking, which in turn may consume more power.

Another problem with the power to be scavenged is that it can be less than the power required to power the switching/oscillating/optimizing scavenging electronics. This can make it feasible to integrate the driver electronics with the original electronics, since these applications already are highly power optimized. When this is not possible, a separate driver has to be constructed as interface. A custom IC for harvesting energy from RF was designed and manufactured, which is reviewed here [23]. The IC has an on-chip MOSFET transistor, and can with few external components be used in a boost or buck-boost converter design. With the two built in oscillators, the switching can be set to optimize the power output. The IC was tested, and showed together with a rectenna to be able to give useful energy to a battery at input power down to 1µW. This excludes the power used by the boost converter itself, which here was powered from the output of its own converted energy. In order to provide a more efficient power optimum tracking, it was used with an ultra-low power Texas Instruments MSP430 microcontroller, carrying a look up table with predetermined optimum values to set the switching which are fed to the custom IC.

The IC was constructed with the intention to charge a small battery with a voltage in the region 2.5V-4.15V, and intended for input power levels 1µW-250µW. The boost efficiency was 30% at 1.5µW, and leveled out at 60%-70% for input power above 30µW.

Though it was developed with the intention to be used for RF scavenging, it can be used in different scavengers too, showing that it is possible to have a converter useful down to input power of 1µW.

A way to decrease power consumption, is to operate in very low voltage.

The rest of this section will describe sub threshold-voltage operated electronics [24]. The threshold is defined to 400mV. In this ultra-low voltage domain, the possibilities of decreasing energy consumption per instruction executed is investigated for different instruction set architectures.

When considering what program parts is needed in health monitoring systems, it can be concluded that many of the existing commercial super-threshold microcontrollers have way more processing power than needed for the most common low- to mid-bandwidth algorithms used in sensor networks, which of many are used for human health monitoring [24]. This makes the investigation of the sub threshold region interesting. It was found that a design running at 230mV with a 168kHz clock still has more than 4 times the processing power needed for the worst case real time computation of health monitoring.

The working principle in the sub threshold region is worth a short description. In the super threshold region, power consumption will decrease approximately quadratically with the voltage decrease. In the sub threshold region this is not the case. It is reported that standard CMOS gates can operate well below the threshold voltage, sometimes as low as 100mV. And by using conventional CMOS based implementations for more sensitive components, the possibility to decrease the overall power consumption potentially rises.

Consider a CMOS inverter. In the super threshold region, CMOS gates effectively works as switches. With the input high the PMOS is in cut-off and the NMOS is strongly conductive, resulting in 0V at the output. The NMOS can then supply a current I_{on}, and the PMOS has a small leakage current I_{off} referred to as the sub threshold drain-to-source off current. This leakage current is too small to influence the logic functionality of the gate, due to the relative magnitudes of the currents I_{on}/I_{off}, being of the order 10000 or greater. If the supply voltage is below the threshold level, both transistors are in the cut off region (regardless of the input). The leakage current depends exponentially on V_{GS}, and will with current technologies increase one order of magnitude for every 100mV of V_{GS}. So for example with $V_{GS}=200\text{mV}$ the I_{on}/I_{off} ratio is of the order 100. This can in most cases be considered being close to rail voltage and the logic function remains. It has been shown that minimum supply voltage for correct logic function is approximately 50mV for current technologies.

There exists a minimum supply voltage under which the circuitry does not function properly. Factors that affect this limit include sensitivity to process variations, soft error strikes and robustness of the memory. However it is not obvious that an as low voltage as possible will mean the least power consumed. The reason to this is that the clock speed decreases with decreasing supply voltage; the clock cycle time increases. When consider the energy used per clock cycle the leakage current will scale up with increasing clock cycle, creating an optimum power point.

Discussion

This section has briefly studied some state of the art electronic solutions that can be used to build a scavenger. The main problem with constructing such electronics is that the available amount of power often is very low. It is desired that the scavenger itself not consumes any large portion of the available power. Therefore it has to be built with very high demands on its own power consumption. This section has showed that this is possible to do, with switching converters being able to convert down to 1μW. So even if the power amount available is very low, it can still be possible to collect and store it.

Conclusions

This report has put together information usable to evaluate the possibility of using energy scavenging for powering medicinal implants. The most important result are summarized here.

In the case of motion, a mathematical expression for the power extracted from a moving spring-mass system was derived along with a review of real generators tested for human conditions.

- The power extractable from a system with proof mass m, subjected to acceleration a at angular frequency ω is

$$P_{max} = \frac{1}{2} m \frac{a^2}{\omega} Q \quad . \tag{21}$$

  The theoretical maximum output from a scavenger on a human body at the head or chest area is appropriate 2mW per gram of proof mass.

- Motion spectral density for human walking peaks at 1-1.5Hz.
- Generators have proved to be able to scavenge $0.1\mathrm{mWcm}^{-3}$, at walking pace.

The feasibility of harvesting electromagnetic radiation in the radio frequency spectrum was determined by real-world measurements along with the performance of the subsequent rectenna.

- Expected power densities from the GSM 900 and the GSM 1800 band, a distance 25-100m from nearest base station, are $0.3\mathrm{mW}/m^2$ to $3\mathrm{mW}/m^2$ in total.
- A WLAN router can transmit at most 25mW at 2.4GHz.
- Expected power level in an office from a WLAN is of the magnitude $1\mu\mathrm{W}/m^2$.
- Rectennas can be constructed to usefully harvest power densities down to $1\mu\mathrm{W}/cm^2$.

As for scavenging for energy from light, the power density at different

circumstances was evaluated. With the efficiency of commercial solar cells reaching 19%, the possible outcome was predicted. The maximum power point tracking was explained, and examples of a scavenger functionality was given.

For the thermoelectric generator, the generator was mathematically modeled, and reviewed by its performance for assumed conditions on a human.

- The maximum extractable power from a thermoelectric generator with Seebeck coefficient α , internal resistance R_{in} at an applied temperature difference T_{TEG} is $P_{L,max} = \frac{\alpha_{pn}^2 \Delta T_{TEG}^2}{4R_{in}}$ (36)

- The efficiency of the tested generators were of the form

  $\eta = k * \Delta T_{TEG}$ (40)

  with k of the magnitude $0.4 * 10^{-3}$

Section II. A scavenger circuit

To make this work complete and to keep it from getting too theoretical (and to keep the author on the right track), it was decided that a small scavenging circuit should be constructed as a part of it. One or some scavenging methods should be chosen, and using some reasonable cheap electronics a scavenger should be built that collects and stores ambient energy. The most mature and most promising method was found to be to scavenge for energy from light.

A small project started, with the goal to collect as much energy as possible from a given cheap solar cell. The concept earlier found universal of using a large capacitor, a so called supercap, to store the energy was decided to be implemented. To accomplish this some form of intelligent IC was needed as well as the use of a switching DC-DC converter.

Components

The general nature of energy scavenging is difficult mainly of two reasons. The first is that with a varying source of energy, some form of dynamic power point tracking (PPT) needs to be implemented. The second is that most scavenging methods only delivers very low voltage and power. But in the case of solar cell based scavenging this can to some degree be avoided by careful choice of solar cell parameters, as will be shown here.

It was not an option to do an own ASIC construction. And since some form of intelligence was required, a low power microcontroller unit (MCU) was decided to be used. After some search for MCU with low power options, the AVR Attiny13V was picked. It is commercially available as a low power 8-bit MCU, supporting 120 different instructions and have a 1KB flash program memory and 64KB internal SRAM. The most important feature of the MCU was its support for different sleep-modes, in which it does not perform any instructions but rather stays in a very low power passive mode. Its specified operating voltage was 1.8V-5.5V. The one used during the following development was in DIP8 package.

In the setup, a light emitting diode, LED, was used as power source to the

solar cell. It was a randomly selected power LED mounted on an aluminum heat sink, which allows for a large range of illumination levels. The emitted light was white with a color temperature of 3000K. See section III under attachments for a picture of the setup.

The most important properties of the solar cell were specified to the following two. Its voltage span should not exceed the operating voltage of the MCU, and it should provide a usable amount of current at the lowest MCU lowest operating voltage. In Fig 11 below is listed the open circuit voltage and the corresponding short circuit current for that voltage. Due to the nature of the exponential function the resolution at low values is hard to read. Hence, in order to be easy read the graph is split in two.

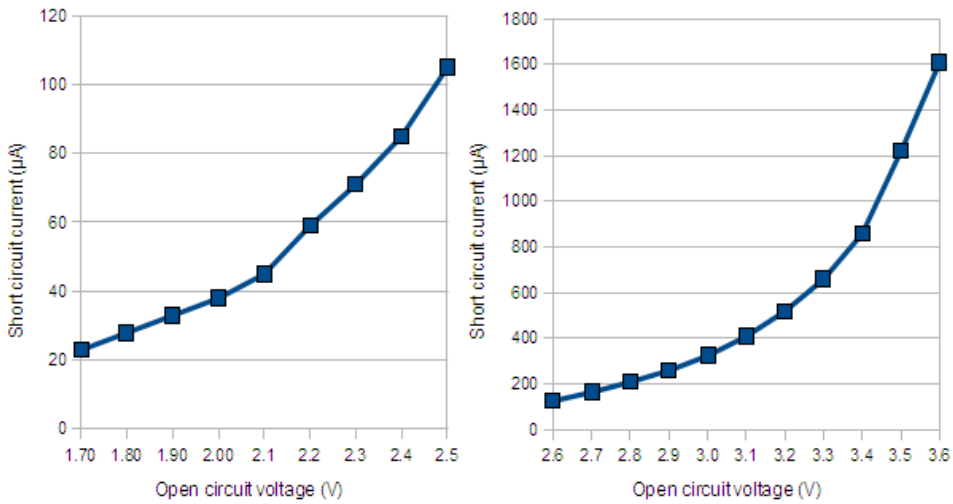

Fig 11. Short circuit current (µA) as a function of the open circuit voltage at the same illumination for the chosen solar cell. Graph split in two to better show the magnitudes of the exponential function.

It is fundamental to understand that involved voltages can differ quite much. At system start up, the solar cell open circuit voltage can be in the range 1.8V~3.7V and the supercap at 0V. Later the supercap can have up to 5V, with the solar cell still in the same region. This large variation demands the use of a switching converter, not only to get reasonable efficiency at low supercap voltages, but to at all be able to boost the input voltage. For this project a DC/DC converter with discrete components, consisting of a traditional buck converter merged with a boost converter was used. The

individual operation of these are shown in Fig 12. Field effect transistors were chosen as realization of the switches to avoid the voltage drop across the p-n junction in the bipolar transistor. The ones selected was specified to work at low voltages, and on top of that the batch was searched for the ones with an especially low threshold voltage. See the circuit diagram in Fig 13, and components used in Table 6.

In section III is attached a picture of the scavenger hardware soldered to an experiment board.

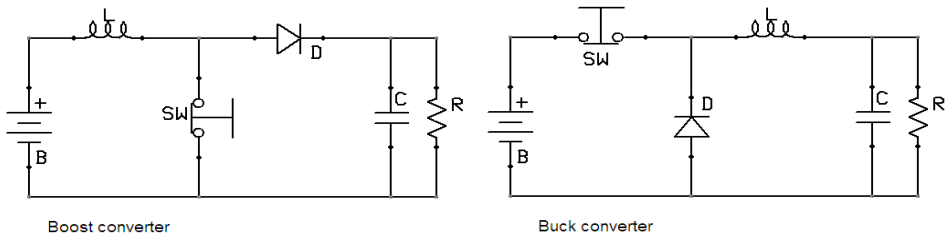

Fig 12. Schematics over the boost and buck converters, switching converters that uses the reactive coil (L) to intermediate store the transferred energy from the DC source (B). When the switch is closed, the source gets drained and the energy which is stored in the coil. When the switch then is opened the coil will continue to force a current through the diode. The boost converter is used to obtain a higher voltage in the load (C R) than in the source. That is often called stepping up the voltage. The buck converter instead steps down the voltage. By good switching technique and appropriate components a high efficiency is achieved.

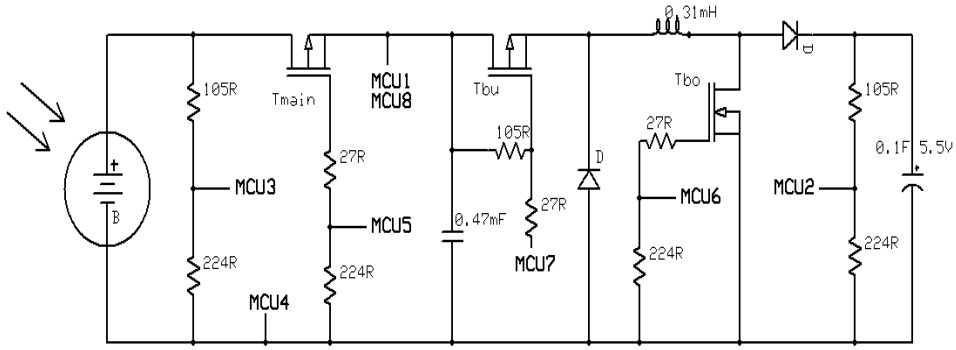

Fig 13. Circuit diagram of the proposed scavenger. Diagram excludes the MCU and only show its connections. Ie MCU2 is pin 2 of the DIP8 IC which is the bidirectional Port3, here used as ADC for the supercap. High impedance voltage dividers are used for less power bleeding. All transistors have their start conditions passively pulled to its desired level, and the reset routine of the MCU actively sets those value to the same.

Component	Kind	Type	Properties
T_{main} , T_{bu}	P-CH MOS-FET	Si3441DV	-0.8V threshold, SSOT-6 package
T_{bo}	N-CH MOS-FET	NDS9956A	1.7V threshold, SO-8 package
D	Schottky diode	10BQ060	60V, 1A rated. 0.5µA reverse current at -5V. Less than 0.4V forward drop at sub 100mA.

Table 6. Data for the components in Fig 12.

Working principle

The most important aspect of the operation is to spend as much time in sleep mode as possible. In active mode, the AVR MCU consumes ca 150µA-300µA by itself, depending mostly on operating voltage. This is clearly more than the solar cell can deliver at many illuminations. So in order to at all be able to work at these low levels, the use of an intermediate buffer is needed, which can provide the needed current in active mode. This opens for the MCU to operate for a short time while draining the buffer and

the buffer recharges while the MCU is sleeping. The least current the MCU can consume in a self waking sleep mode is 5µA, with the watchdog timer set as the self waking interrupt.

The MCU has an on-circuit AD converter with a 1.1V reference. The internal reference allows for measuring its own operating voltage within its whole operating area. Doing this is essential to be able to perform MPPT. The maximum power point, MPP, is modeled as a voltage band, instead of the theoretical working point. With a certain time interval the solar cell's open circuit voltage is measured. Since the MCU does this measurement in intervals it can handle varying light conditions. The measurement is done by releasing the loading of the cell with a PMOS transistor while the MCU takes power from the intermediate buffer. From this value it has through testing been found that the MPP is at roughly 85%-90% of the open circuit solar cell voltage. Draining of the solar cell close to this point hence means it's approximately being optimally loaded. In software is calculated an upper and a lower limit, defining the band. When the voltage reaches the upper limit the MCU is allowed to start up and transfer power. When the voltage has fallen down to the lower limit it will go into sleep waiting for the intermediate voltage to build up again to the upper limit. While asleep the MCU will make short wake-ups to check if the voltage is high enough. The typical sleep time is 125ms. The mean power consumption in this voltage build-mode will be low. Hence a high efficiency is obtained here. The program flow is summarized in Fig 14.

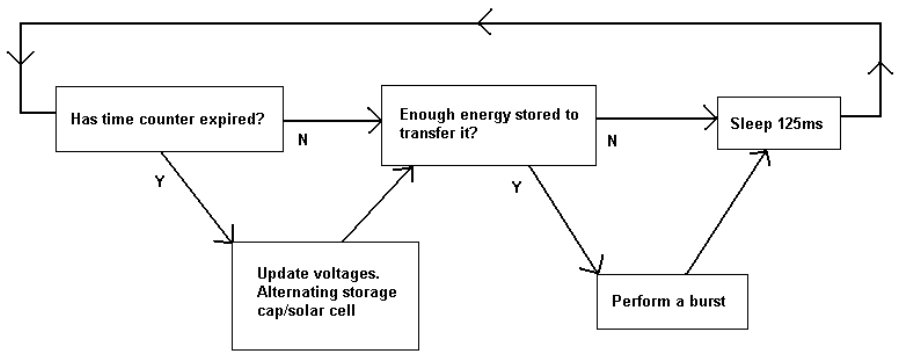

Fig 14. Flow chart for the software algorithm.

While awake, the MCU will consume a significant part of the supplied current. Because of this it is desired to spend as little time as possible in that mode. During the time awake it will either perform a buck or a boost burst, transferring energy from the intermediate buffer to the supercap. It is desired to transfer as much energy as possible during this time. Because by doing that the efficiency can be made high also in this drain-mode and the problem with the proportional large power consumption of the MCU is avoided. If this technique makes the efficiency in this mode acceptable, that makes for the overall efficiency to be quite good, at least in theory.

The voltage of the supercap is also measured with a certain time interval. This way the MCU can determine a good pulse quote for the switching converter as well as which mode (buck or boost) should be used. Depending on the both voltages, the MCU will go through several different steps to always charge the supercap at the highest possible rate. The maximum rating of the supercap is 5.5V, why the charge terminates at 5V.

In Fig 15 below is captured a full run. A picture of the experimental setup is found in the appendix. The supercap voltage is the blue curve, start from 0V and charges to full on 5.0V. The red curve is the voltage of the intermediate buffer, the 470µF capacitor in Fig. This curve is seen varying in a band of approximate constant size. When the supercap voltage stops rising the scavenger stops loading the solar cell. This can be seen by the voltage on the intermediate buffer reaching the solar cell open circuit voltage (constant). The band visualizes the approximate MPP, which is set to 85%-90% of the solar cell open circuit voltage. The different modes the scavenger goes through depends on the both voltages. In this run only the light is set at a constant level. Small changes in the way the intermediate buffer drains can be seen, giving a hint of when a mode change occurs.

For demonstration purpose a smaller 6.8mF capacitor has been used as supercap. Unfortunately some discretization error occurs, mainly on the red curve.

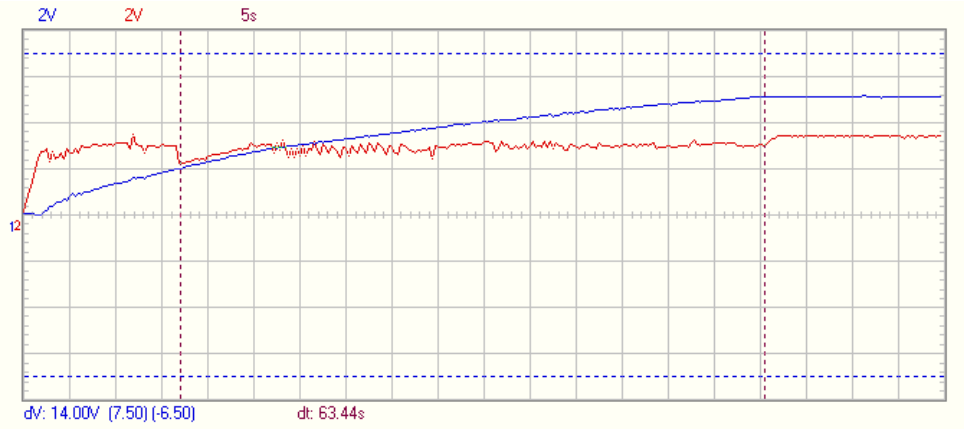

Fig 15. Typical run from 0V at supercap to 5.0V and constant illuminance. Blue curve shows voltage building up square root-like on the supercap. Red curve shows the voltage at the intermediate cap, laying close to the MPP. At second marker the supercap is full and the circuit stops loading the solar cell, resulting in its open circuit voltage ending up at the intermediate cap. A smaller 6.8mF capacitor is used as supercap to acquire a faster run, but doesn't change the curve forms. One horizontal square is 5seconds, one vertical is 2V. Zero voltage level is at the marked horizontal center line.

Up till the first vertical marker the scavenger goes through two different buck modes that change the pulse quote to keep charging the cap effectively. When it finds the cap voltage has built enough to be safe to "lock on to" (ie it is at least the minimum operating voltage of the MCU) it opens T_{bu} instead of switching it. When it finds that this isn't effectively anymore it starts to boost the voltage by giving bursts to T_{bo} .

This whole time the operating principle is to start a switching when the intermediate voltage has built enough. At the second vertical marker in Fig 15, the stored voltage has reached 5.0V. The charging is then terminated. At this point it is visible how the intermediate voltage builds up to the solar cell open circuit voltage since this is no longer loaded, and T_{bu} is open. This demonstrates how the scavenger operates at a voltage band close around the calculated MPP.

The measurement of the solar cell open voltage is done with two measurements, and then the mean is taken. The time between these measurements is chosen so that the scavenger will try to compensate for 100Hz indoor light flicker.

The following Fig 16 is a short time recording of the voltage at the intermediate cap during operation. It shows the principle of the voltage building up while the MCU sleeps, and then quickly give a burst that drains the intermediate stored energy. The total variation within the vertical markers is the modeled MPP band.

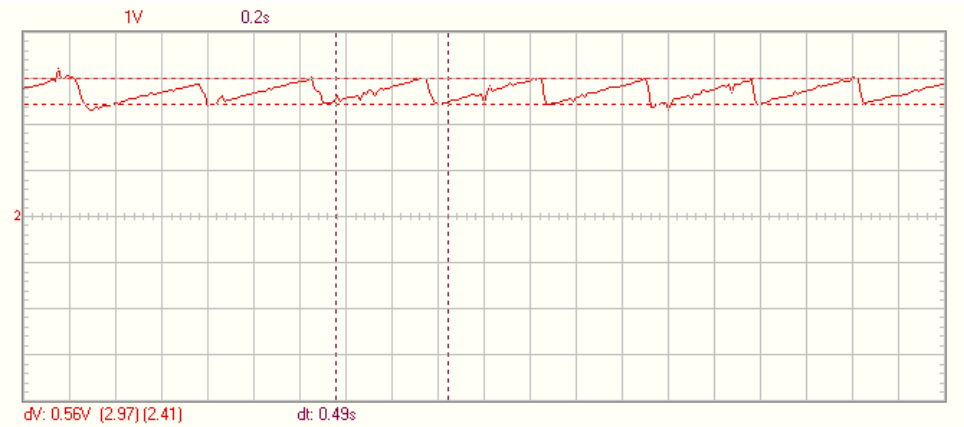

Fig 16. Voltage on intermediate cap as a function of time. With the MCU in a sleep mode the voltage builds up. When the voltage reaches the MPP upper limit, it gives a quick burs and transfer a part of the stored energy to the supercap. Burst time is typical 20ms in this recording. One horizontal square is 0.2s and one vertical is 1V. Data is somewhat noisy due to the switching.

Performance

It was desired to make the circuit perform as good as possible. This is a quite vague goal, so in order to specify it in more detail the following aim was set. The circuit should charge a capacitor faster at a fix illumination than the solar cell would do coupled directly to it. This means, if succeeded, that there is a positive tradeoff for the added power consuming intelligence. There is also the benefit of the boosting possibility.

One easily overlooked concern is that care has to be taken while charging between capacitors (which is what the scavenger does). If two capacitors are connected, having different initial voltage, then electrical energy will be lost. Let's revisit some basic relations to show this more precise. The

capacitance

$$C = Q/V \tag{43}$$

and the energy in C_k charged to V_k is

$$E_k = 0.5 * C_k * V_k^2 \quad . \tag{44}$$

When connecting charged capacitors together, the total amount of charge remains unchanged. Assume two capacitors are connected,

$$Q_{tot} = Q_1 + Q_2 = C_1 V_1 + C_2 V_2 \quad . \tag{45}$$

Putting two capacitors in parallel adds the capacitance's to get the total. The voltage after the coupling can be written

$$V_{tot} = \frac{C_1 V_1 + C_2 V_2}{C_1 + C_2} \quad . \tag{46}$$

The stored energy in both capacitors before and after the coupling hence is

$$E_{separate} = \frac{1}{2} C_1 V_1^2 + \frac{1}{2} C_2 V_2^2 \tag{47}$$

and

$$E_{toghether} = \frac{1}{2}(C_1 + C_2)\left(\frac{C_1 V_1 + C_2 V_2}{C_1 + C_2}\right)^2 = \frac{1}{2}\frac{(C_1 V_1 + C_2 V_2)^2}{C_1 + C_2} \quad , \tag{48}$$

respectively. These equations aren't trivial to interpret. But by putting some numbers in the expressions above it becomes clearer. If two equal large capacitors are coupled together, with one of them having 0V, and the other some volt V , it follows that half the originally stored energy will dissipate because of the connecting. Each capacitor will consequently have one forth of the original energy mutually stored.

This hopefully helps to explain why it is a tricky problem to scavenge for energy in the proposed way with two capacitors, with one transferring charge to the other. Also the need for a switched converter in between becomes obvious, since storing the energy in a third reactive element is a must to avoid the above described source of losses.

Since the energy in a capacitor depend quadratic on the voltage, the voltage build should ideally follow a square root function at a constant input of energy. A constant input-rate of energy is obtained from a solar cell if it is

kept at its MPP. On the contrary, if the solar cell is connected directly to the capacitor, voltage will first increase approximately linear, due to the solar cell acting as a constant current source, with the current being proportional to the illumination. When the solar cell has charged the capacitor to close its open circuit voltage, it will level off quite direct. This can be seen in Fig 17, where it is showed next to the how the designed circuit behaves for the same conditions. Compare with the multiple curves in Fig 7.

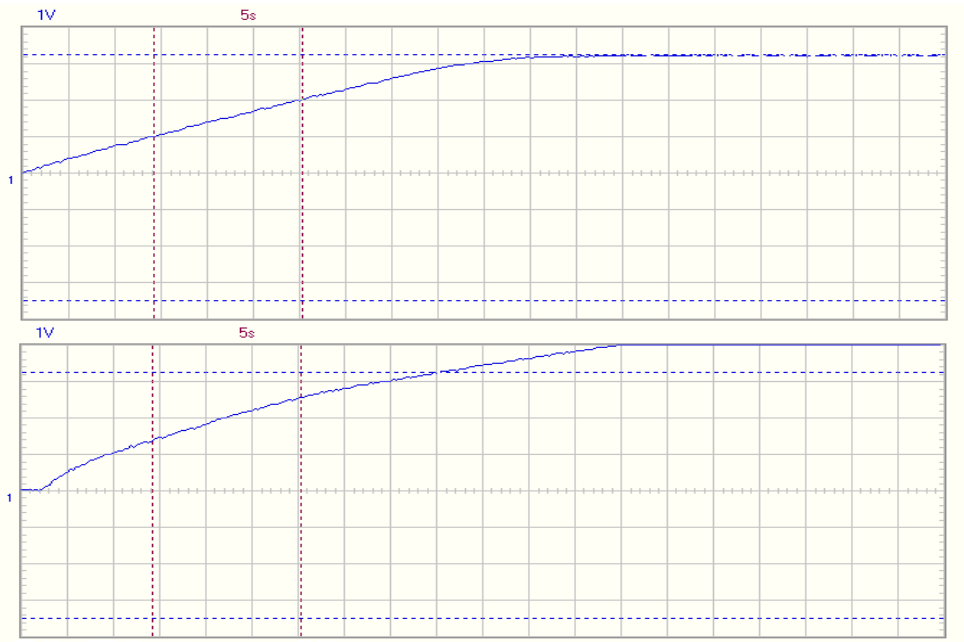

Fig 17. Comparison, passive cell connected to supercap (above) vs the scavenger operating (below) for the same conditions. The active circuit is clearly faster to 1V, 2V and 3V. After having passed the solar cells voltage it continue to boost the voltage out of range of the scope. In fact, the time base was chosen to just end when the cap reaching 5.0V for the active scavenger.

The scavenger charges the supercap faster to any voltage faster than the solar cell does when coupled directly to it. Hence the scavenger is considered to have achieved its goal. Note that the square root-likeness is there, which suggest that the scavenger indeed does transfer energy at a constant rate. There is a positive tradeoff for the added circuitry. The

recording is started in the same moment as the circuits were powered on. The active one keeps the supercap voltage at 0V for ca half a second before it starts to charge, which is explained by the intermediate voltage needs to rise to a certain level before there is enough stored energy to make a burst.

The relatively weakest part of the active circuit is around where the supercap voltage is close to the solar cell's MPP. This is seen by the derivative of the active curve being slightly less than the passive one. This is naturally, since the added circuitry only can lessen the power transfer in this region due to its own power consumption. The solar cell is close to its MPP, and will hence passively perform optimal. As seen earlier, the scavenger tries to compensate for this by "locking on" to the solar cell in this region, and hence performs as little work as possible. Despite this, the effect is visible for some light conditions, as in the case of Fig 17.

Improvements

Though the scavenger is considered to have achieved its goal of outperforming the passive solar cell, there is room for improvements. Here follows a few points.

Without changing the concept, a more power efficient architecture could be used. An example is the Texas Instruments MSP430 family. Its members can operate at lower voltages and have in general a factor 2-10 less own power consumption. Especially lower power consumption in sleep mode can increase the working area of the scavenger.

Moreover, the voltage dividers to the AD converter could be turned on/off with a MOSFET, so that they only bleed power during the short conversion time. This was however not possibly on the used Attiny13V due to shortage of pins. In the proposed design the supercap will bleed approximate 20µW in the voltage divider. Since the scavenger starts to operate at less than 40µW this is obviously a limiting factor.

A better supercap would furthermore increase the performance. Less series resistance will allow for a higher rate of energy transfer in the bursts, cutting down on the average energy consumed by the MCU. A higher parallel resistance will decrease the power bleeding.

The design is also rather bulky due to the large low resistance inductor. Also the hardware design is obviously made without regard to the EMC and

ESD regulations, making it unfit at this stage for commercial use.

Conclusion

A complete scavenger has been designed. Based on the study of scavenging methods from section I, the solar cell approach was found to be the most feasible and was hence chosen. The algorithm of having two operating modes proved to be usable, one while mostly sleeping consuming very little power, and one where a portion of energy is transferred. This algorithm is generic and can be used for other input sources, as long as the source can push the intermediate voltage above the MCU threshold operating voltage. Though with different magnitudes involved, the algorithm details needs to be reviewed. This includes sleep times and component values.

As for the hardware it is clearly not intended for any medical application. To do this in a proper way was outside of the scope of this project, and focus was put at evaluating the algorithm.

Section III

References

[1] A. Khaligh, P. Zeng, X. Wu, Y. Xu, “A hybrid energy scavenging topology for human-powered mobile electronics”. Electrical and Computer Engineering Department, Illinois Institute if Technology.

[2] E. Romero, R. O. Warrington, M. R. Neuman, “Body motion for powering biomedical devices”. 31st Annual International Conference of the IEEE EMBS Minneapolis, Minnesota, USA, september 2-6, 2009.

[3] M. Renaud, T. Sterken, P. Fiorini, R. Puers, K. Baert, C. van Hoof, “Scavenging energy from human body: Design of a piezoelectric transducer”. Katholieke Universiteit Leuven, Belgium.

[4] B.J. Bowers, D.P. Arnold, “Spherical, rolling magnet generators for passive energy harvesting from human motion”. Interdisciplinary Microsystems Group, Department of Electrical and Computer Engineering, University of Florida, USA.

[5] Venkateswara Sarma Mallela, V Ilankumaran, N. Srinivasa Rao, “Trends in cardiac pacemaker batteries”. Available: http://www.ncbi.nlm.nih.gov/pmc/articles/PMC1502062/ [February 15th, 2011]

[6] H. J. Visser, A. C. F. Reniers, J. A. C. Theeuwes, “Ambient RF energy Scavenging: GSM and WLAN power density measurements”. Holst Centre and TNO Science & Industry, The Netherlands.

[7] J. A. Hagerty, T. Zhao, R. Zane, Z. Popovic, “Efficient broadband RF energy harvesting for wireless sensors”. Department of Electrical and Computer Engineering, University of Colorado at Boulder.

[8] Post- och telestyrelsens författningssamling. Available:

http://www.pts.se/upload/Foreskrifter/Radio/PTSFS-2008-04-undantagsforeskrifter-vissa-radiosandare.pdf [may 1st, 2011]

[9] S. A. Bhalerao, A. V. Chaudhary, R. B. Deshmukh, R. M. Patrikar, “Powering wireless sensor nodes using ambient RF energy”. 2006 IEEE International Conference on Systems, Man and Cybernetics.

[10] G. Akram, Y. Jasmy, “Lab VIEW-based planar multilayered model for estimation of the absorbed energy inside biological tissues”. Faculty of Electrical Engineering, Technology University of Malaysia.

[11] G. Kang, O.P. Gandhi, “Effect of dielectric properties on the peak 1- and 10-g SAR for 802.11 a/b/g frequencies 2.45 and 5.15 to 5.85 GHz”. IEEE transactions on electromagnetic compatibility, May 2004.

[12] N. Dorababu, Y. Ratna Kumar, K. Venkatesu, G. Karunakar, G.S.N. Raju, “Electromagnetic energy in biological tissues”. Department of Electronics and Communication Engineering, Visakhapatnam, India.

[13] J. Kho, “Whats behind record breaking solar cell efficiencies”. Available: http://www.electroiq.com [March 3rd 2011]

[14] First solar, Inc. Available: http://www.firstsolar.com [April 4th, 2011]

[15] A. Gustafsson, “ Komponentfysik”. Fasta Tillståndets Fysik, Lunds Tekniska Högskola, 2008.

16] H. Shao, C. Tsui, W. Ki, “An inductor-less MPPT design for light energy harvesting systems”. Department of Electronic and Computer Engineering, The Hong Kong University of Science and Technology.

[17] Physikalisch-Meteorologisches Observatorium Davos Available: http://www.pmodwrc.ch/pmod.php?topic=tsi/composite/SolarConstant [April 4th, 2011]

[18] Johan Moan, “Visible light and UV radiation”. Available: http://www.uio.no/studier/emner/matnat/fys/FYS3610/h04/undervisningsmateriale/Moan7.pdf [April 4th, 2011]

[19] The Engineering toolbox, “Illuminance – Recommended Light levels”. Availabel: http://www.engineeringtoolbox.com/light-level-rooms-d_708.html [April 4th, 2011]

[20] S. Dalola, M. Ferrari, V. Ferrari, M. Guizzetti, D. Marioli, A. Taroni, “Characterization of thermoelectric modules for powering autonomous sensors”. IEEE Transactions on Instrumentation and Measurements, January 2009.

[21] Z. Wang, V. Leonov, P. Fiorini, C. van Hoof, “Micromachined thermopiles for energy scavenging on human body”. IMEC vzw and Katholieke Universiteit Leuven, Belgium.

[22] L. Carlioz, J. Delamare, S. Basrour, G. Poulin, “Hybridization of magnetism and piezoelectricity for an energy scavenger based on temporal variation of temperature”. Micro and Nano Systems Group, Grenoble, France and MagMems-G2ELab, St martin d'Hères Cedex, France.

[23] T. Paing, E. Falkenstein, R. Zane, Z. Popovic, “Custom IC for ultra-low power RF energy harvesting”. Colorado Power Electronics Center.

[24] L. Nazhandali, B. Zhai, J. Olson, A. Reeves, M. Minuth, R. Helfand, S. Pant, T. Austin, D. Blaauw, “Energy optimization of sub threshold-voltage sensor network processors”. The University of Michigan.

Appendix

1. Scavenger hardware

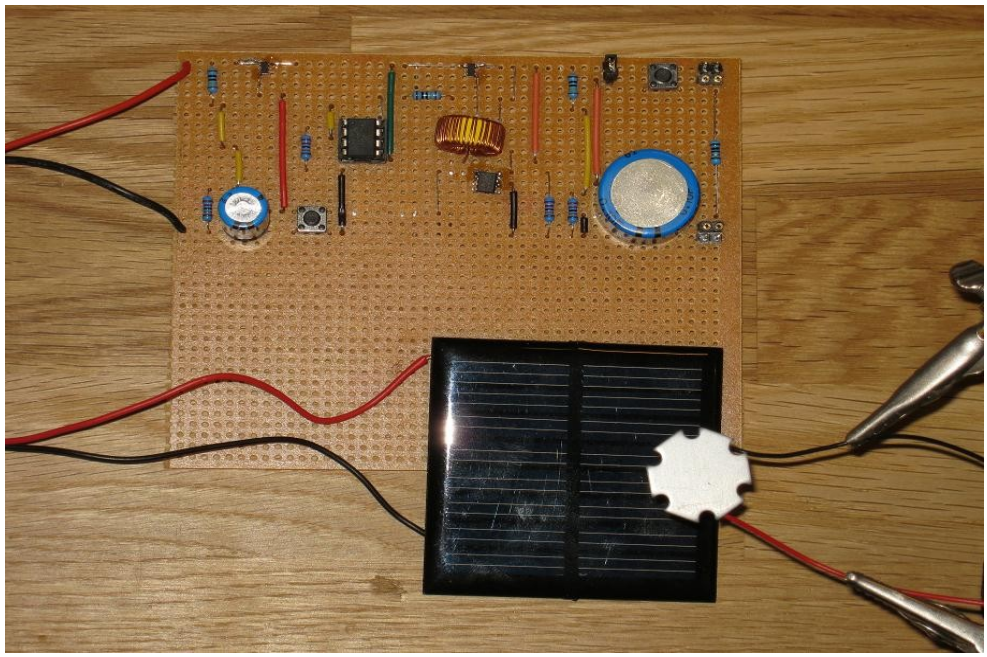

Fig 18. The experimental setup used in section II. A power LED lighten the used solar cell which gives its input to the scavenger soldered to an experiment board. The solar cell U-I characteristics did not change for different color temperature of the LED.

2. Scavenger board closeup

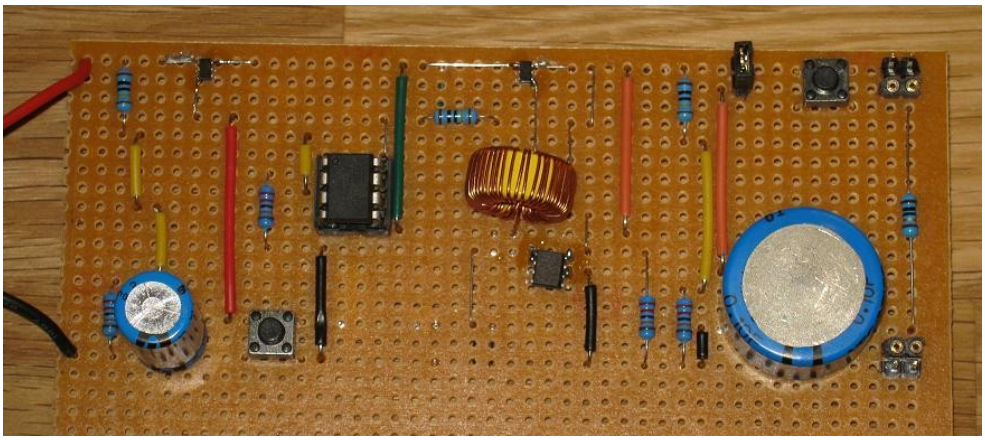

Fig 19. Board closeup. Components placed roughly as in the schematic. Few additional components added for easy measurements and discharging.

3. Scavenger board backside

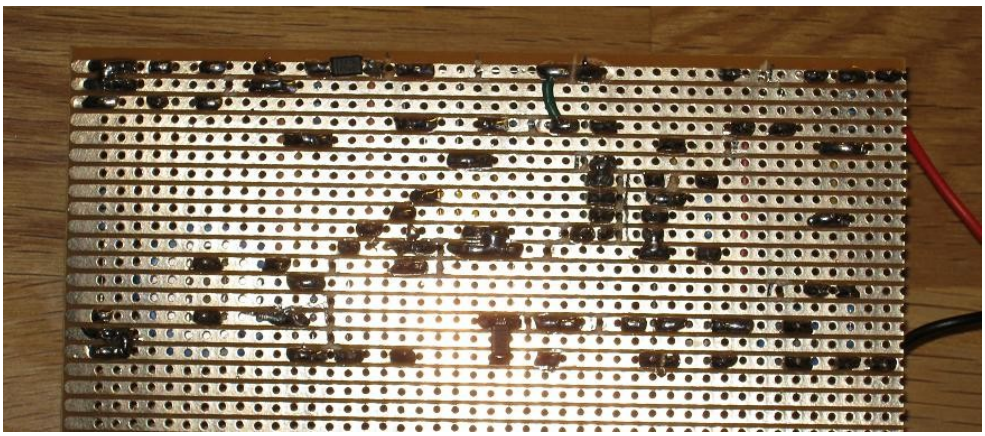

Fig 20. Backside of board.. The only two components are the surface mounted diodes.

4. Source code

```
;************************** Solar scavenger **********************
;This project is a scavenger circuit, maximizing the output from a
;solar cell. The power is stored in a 0.1F 5V cap.
;For the "Energy svangenging" thesis.
;v2.45

;Main clk 4.8MHz, internally divided by 8.



;Hardware config:
;Solar cell coupled in parallel with 0.47mF after Tmain.
;Pin: function
;1: RST, dnc/VCC
;2: PB3 ADC3 input from divided cap
;3: PB4 ADC2 input from divided s.c. voltage
;4: GND
;5: PB0 output, Tmain         PMOS
;6: PB1 output, Tboost        NMOS
;7: PB2 output, Tbuck         PMOS
;8: VCC

;Real voltage ~= 24.4e-3 * adc number



;To program TN13 with STK500: RST@PE 2 PB5 ^ XT1@PE 2 PB3.



.include "tn13def.inc"
```

```
.def Temp = r16                 ;Universal temporary registers
.def Temp2 = r17
.def Temp3 = r18
.def Voltage = r19              ;Present voltage
.def Time = r20                 ;Time counter

;Define memory constant's place in SRAM
.equ SC_voltage = 0x60              ;Present s.c. open voltage
.equ CAP_voltage = 0x61             ;Present cap voltage
.equ Last_was_solar = 0x62          ;1 if last adc was from solar cell
.equ Upper_voltage = 0x63           ;This is the dynamic upper limit for MPP
.equ Lower_voltage = 0x64           ;This is the dynamic lower limit for MPP
.equ Mode       = 0x65              ;Specify mode, buck/boost and pulse quote

;Constants used. All has been tested for optimization/correctness
.equ Switching_periods = 100    ;A constant used when switching
.equ Time_max = 10              ;Divide by 10 gives approx #s between updates
.equ Voltage_difference = 7     ;If Vcap + this > Vsc then boost mode.
.equ Vcritical = 73             ;Absolute minimum operating V for µC
.equ Vfull = 213                ;5.0V, maximum of cap


.cseg

;Define interrupt vectors
.org 0
rjmp RESET
.org 8
rjmp WATCHDOG           ;Watchdog Interrupt Handler
.org 9
```

```
rjmp ADC_COMLETE          ;ADC Conversion Handler


.org 10

RESET:

;Tmain conducting: 0, Tbo cut-off: 0, Tbu cut-off: 1. Aslo passively set
in HW
ldi Temp,0b00000100
out PORTB,Temp

ldi Temp,0b00000111               ;Data direction bits, read/write
out DDRB,Temp

ldi Temp, low(RAMEND)       ;Set stack pointer
out SPL, Temp


;Configure interrupts:

;WDT reset
ldi Temp, (1<<WDE | 1<<WDCE)             ;Reset WDT
out WDTCR,Temp
ldi Temp, (0<<WDE)
out WDTCR,Temp

;Comparator disable to save power. Default on = 0
ldi Temp,(1<<ACD)
out ACSR,Temp
```

```
;Clear all registers
clr r16
clr r17
clr r18
clr r19
clr r20
clr r21
clr r22
clr r23
clr r24
clr r25
clr r26
clr r27
clr r28
clr r29
clr r30
clr r31

sei             ;Interrupts active


;*********************************************************************
;*********************************************************************
;*********************************************************************


;Measure both voltages and set all parameters (slowly).
rcall GO_SLEEP_125ms
```

```
;Start by checking if high enough voltage,
;set mux to s.c. MUX2 @ PB4, wait and make ADC
ldi Temp, (1<<ADLAR | 1<<MUX1 | 0<<MUX0 | 1<<REFS0)       ;Use internal Vref
out ADMUX,Temp
rcall GO_SLEEP_16ms          ;Short mux settling time
rcall GET_ANALOG
cpi Voltage,Vcritical
brcs RESET                   ;Dont try to start if very low voltage

rcall TO_SOLAR_CELL          ;Get solar cell voltage

rcall TO_CAP                 ;Get supercap voltage

MAIN:                        ;Main loop

rcall CHECK_TIME             ;Time to update sc/cap data?

rcall RUN

rcall GO_SLEEP_125ms

rjmp MAIN


;*****************************************************************
;*****************************************************************
;*****************************************************************


CHECK_TIME:
```

```
;This routine checks the total time elapsed, estimated from adding
;in sleep routines. If time expired then update data from
;alternating storage cap/ solar cell.

cpi Time,Time_max
brcs NOT_TIME_YET

clr Time              ;Time = 0

LDS Temp,Last_was_solar
cpi Temp,1
breq TO_CAP
rjmp TO_SOLAR_CELL

TO_CAP:

ldi Temp,0
STS Last_was_solar,Temp

;Set mux to cap MUX3 @ PB3, wait and make ADC.
ldi Temp, (1<<ADLAR | 1<<MUX1 | 1<<MUX0 | 1<<REFS0)      ;Use internal Vref
out ADMUX,Temp
rcall GO_SLEEP_16ms
rcall GET_ANALOG

STS CAP_voltage,Voltage

;Reset mux to s.c. default
ldi Temp, (1<<ADLAR | 1<<MUX1 | 0<<MUX0 | 1<<REFS0)
out ADMUX,Temp
```

```
rcall UPDATE_BB             ;Buck/boost

ret

TO_SOLAR_CELL:

ldi Temp,1
STS Last_was_solar,Temp

;Release s.c, set mux to s.c. MUX2 @ PB4, wait, make ADC, set Tmain
;Do 2 measurements with 16ms between to compensate for indoor light flicker
sbi PORTB,0
ldi Temp, (1<<ADLAR | 1<<MUX1 | 0<<MUX0 | 1<<REFS0)       ;Use internal Vref
out ADMUX,Temp
rcall GO_SLEEP_16ms         ;Let mux settle
rcall GET_ANALOG            ;Get first sample
mov Temp3,Voltage
lsr Temp3                   ;Half the sample
rcall GO_SLEEP_16ms         ;Wait other side of mains period
rcall GET_ANALOG
lsr Voltage
add Voltage,Temp3           ;Voltage mean of high and low mains level
cbi PORTB,0

STS SC_voltage,Voltage

rcall UPDATE_LIMITS

ret
```

```
NOT_TIME_YET:

ret

;*********************************************************************

UPDATE_LIMITS:
;Routine calculate optimal Vlimits for loading
;based on solar cell open voltage. Run once s.c.o.v. are updated.
;Updates memory at Upper_voltage and Lower_voltage

LDS Temp,SC_voltage
cp Temp2,Temp

lsr Temp2
lsr Temp2
lsr Temp2

sub Temp,Temp2
cpi Temp,Vcritical
brcc UPDATE_LIMITS_SKIP_1
ldi Temp,Vcritical
UPDATE_LIMITS_SKIP_1:
STS Upper_voltage,Temp

sub Temp,Temp2
cpi Temp,Vcritical
```

```
brcc UPDATE_LIMITS_SKIP_2
ldi Temp,Vcritical
UPDATE_LIMITS_SKIP_2:
STS Lower_voltage,Temp

ret


UPDATE_BB:
;Update buck/boost relation. Updated when new cap voltage.

LDS Temp,CAP_Voltage
LDS Temp2,SC_Voltage
subi Temp2,Voltage_difference
cp Temp,Temp2
brcc BOOST_MODE

LDS Temp,CAP_Voltage
cpi Temp,Vcritical/3
brcc MID_LEVEL

ldi Temp,0
STS Mode,Temp

ret

MID_LEVEL:

LDS Temp,CAP_Voltage
cpi Temp,Vcritical-10
```

```
brcc MID_LEVEL_2

ldi Temp,1
STS Mode,Temp

ret

MID_LEVEL_2:

LDS Temp,CAP_Voltage
cpi Temp,Vcritical
brcc BOOST_MODE

LDS Temp,SC_Voltage          ;If close to critical on cap and high sc
cpi Temp,Vcritical+10
brcs MID_LEVEL_3             ;TEST FOR LOW SC VOLTAGE

ldi Temp,1
STS Mode,Temp
ret

MID_LEVEL_3:

ldi Temp,2
STS Mode,Temp

ret

BOOST_MODE:
```

```
ldi Temp,3
STS Mode,Temp

ret

;*********************************************************************


GET_ANALOG:             ;Make AD conversion on preselected mux

;Enable ADC. 010 -> 2kSps @4.8/8MHz found lowest power.
ldi Temp,(1<<ADEN | 1<<ADIE | 0<<ADPS2 | 1<<ADPS1 | 0<<ADPS0)
out ADCSRA,Temp
ldi Temp, (1<<SE | 1<<SM0)
out MCUCR,Temp
sleep

in Voltage,ADCH             ;Always return in dedicated register

;Disable ADC and sleep
ldi Temp,0
out ADCSRA,Temp
out MCUCR,Temp

ret

;*********************************************************************
```

```
RUN:
;Checks if voltage built up to optimal limit yet, if so then start
;switching. If not, then sleep to let continue build up.

;Set mux to s.c. MUX2 @ PB4, wait and make ADC
ldi Temp, (1<<ADLAR | 1<<MUX1 | 0<<MUX0 | 1<<REFS0)       ;Use internal Vref
out ADMUX,Temp
rcall GO_SLEEP_16ms
rcall GET_ANALOG
cpi Voltage,Vcritical
brcc RUN_OK

ldi Temp,0b00000100        ;Very low int. cap voltage, set initial conditions
out PORTB,Temp
rcall GO_SLEEP_1s
ldi Temp,10
sub Time,Temp              ;If voltage goes critical then stop counting

ret

RUN_OK:                          ;S.c. voltage not critical low

LDS Temp,CAP_Voltage
cpi Temp,Vfull
brcs RUN_OK2

inc Time                         ;Can afford to update a little faster here

ret
```

```
RUN_OK2:                    ;Cap voltage not too high

LDS Temp,Upper_voltage
cp Voltage,Temp             ;Voltage momentary voltage at sc
brcc UPPER_REACHED

ret                         ;If not reached upper limit then return

UPPER_REACHED:              ;Router routine depending on mode

LDS Temp,Mode       ;Fetch mode
cpi Temp,0
breq DO_BUCK
LDS Temp,Mode       ;Fetch mode
cpi Temp,1
breq DO_BUCK_MID
LDS Temp,Mode       ;Fetch mode
cpi Temp,2
breq DO_SHORT_BOOST
rjmp DO_BOOST


;*****************************************************************


DO_BUCK:

ldi Temp2,200               ;Max times this routine runs
```

```
DO_BUCK_AGAIN:

cbi PORTB,1                    ;Tbo not conducting in buck mode
ldi Temp,Switching_periods/2

DO_BUCK_0:
cbi PORTB,2                    ;Good times with right clk
sbi PORTB,2
nop
nop
cbi PORTB,2
sbi PORTB,2
dec Temp
brne DO_BUCK_0

dec Temp2
brne DO_BUCK_1
ldi Temp,1
STS Mode,Temp              ;Change mode if had to escape this way
ret

DO_BUCK_1:
rcall GET_ANALOG               ;Mux is already correct
LDS Temp,Lower_voltage
cp Voltage,Temp
brcc DO_BUCK_AGAIN
ret             ;To main


DO_BUCK_MID:
```

```
ldi Temp2,100              ;Max times this routine runs

DO_BUCK_MID_AGAIN:

cbi PORTB,1                ;Tbo not conducting in buck mode
ldi Temp,Switching_periods/2

DO_BUCK_MID_0:
cbi PORTB,2
nop
nop
nop
nop
nop
sbi PORTB,2
dec Temp
brne DO_BUCK_MID_0

dec Temp2
brne DO_BUCK_MID_1
ret

DO_BUCK_MID_1:
rcall GET_ANALOG
LDS Temp,Lower_voltage
cp Voltage,Temp
brcc DO_BUCK_MID_AGAIN
ret
```

```
DO_SHORT_BOOST:

cbi PORTB,2                ;Tbu conducting while boosting
ldi Temp,Switching_periods/3

DO_SHORT_BOOST_0:
sbi PORTB,1
cbi PORTB,1
nop
sbi PORTB,1
cbi PORTB,1
dec Temp
brne DO_SHORT_BOOST_0

sbi PORTB,2

ret


DO_BOOST:

cbi PORTB,2                ;Tbu conducting while boosting
ldi Temp,Switching_periods

DO_BOOST_0:
sbi PORTB,1
cbi PORTB,1
nop
sbi PORTB,1
```

```
cbi PORTB,1
dec Temp
brne DO_BOOST_0

ret


;*****************************************************************


GO_SLEEP_1s:

ldi Temp,10
add Time,Temp

ldi Temp,(1<<WDTIE | 1<<WDP2 | 1<<WDP1)        ;110 -> 1s
out WDTCR,Temp
ldi Temp, (1<<SE | 1<<SM1)
out MCUCR,Temp
sleep

ret


GO_SLEEP_125ms:

ldi Temp,1
add Time,Temp

ldi Temp,(1<<WDTIE | 1<<WDP1 | 1<<WDP0)        ;011 -> 0.13s
```

```
out WDTCR,Temp
ldi Temp, (1<<SE | 1<<SM1)
out MCUCR,Temp
sleep

ret


GO_SLEEP_16ms:

ldi Temp,(1<<WDTIE | 0<<WDP0)        ;000 -> 16ms
out WDTCR,Temp
ldi Temp, (1<<SE | 1<<SM1)
out MCUCR,Temp
sleep

ret


;************************ Interrupt routines ***********************


WATCHDOG:
;Start execution here at wake up from sleep. Turns off WDT and returns

push Temp
in Temp,Sreg
push Temp

;Disable WDT
```

```
ldi Temp, (1<<WDE | 1<<WDCE)
out WDTCR,Temp
ldi Temp,0
out WDTCR,Temp

pop Temp
out Sreg,Temp
pop Temp

reti


;*********************************************************************


ADC_COMLETE:

;This just returns to normal execution

reti
```